Chapter 1
Nanostructured Materials for High Efficiency Perovskite Solar Cells

Meidan Ye, Xueqin Liu, James Iocozzia, Xiangyang Liu and Zhiqun Lin

Abstract Capturing renewable energy has become an increasingly urgent task due to concerns over fossil fuel supplies and accessability in the future. Photovoltaic technology represents the most promising strategy to address this problem. However to date, no solar cell module has been able to satisfy the simultaneous requirements of high efficiency, low cost and long lifetime necessary for large scale production and application. Recent development in organic-inorganic halide perovskite solar cells (PSCs) has shown great potential for large-scale application owing to the superb power conversion efficiency (PCE), facile device fabrication and low material cost. Since the first report of methyl ammonium lead halide, $CH_3NH_3PbX_3$ (X = Br, I), sensitized liquid solar cells in 2009, the PCEs of PSCs have jumped from 3.8 to 20.2 %. Research efforts on new preparation processes and materials design for PSCs still remain highly active. This chapter will concentrate on summarizing the recently reported nanostructured materials (i.e. TiO_2, Al_2O_3, ZnO, carbon materials and others) applied in PSCs. This chapter strives to present a comprehensive overview and provide a deep understanding of nanostructured materials in PSC devices.

1.1 Introduction

Increasing energy demands, diminishing amounts of easily-accessible fossil fuel sources, and concerns of global warming have motivated a great deal of effort into the exploration and development of clean, inexpensive and renewable energy

M. Ye · X. Liu
Research Institute for Biomimetics and Soft Matter,
Fujian Provincial Key Laboratory for Soft Functional Materials Research,
Department of Physics, College of Physical Science and Technology,
Xiamen University, Xiamen 361005, China

X. Liu · J. Iocozzia · Z. Lin (✉)
School of Materials Science and Engineering, Georgia Institute of Technology,
Atlanta, GA 30332, USA
e-mail: zhiqun.lin@mse.gatech.edu

Q. Li (ed.), *Nanomaterials for Sustainable Energy*,
NanoScience and Technology, DOI 10.1007/978-3-319-32023-6_1

sources [1]. It is important to note that research into alternative and renewable energy resources is motivated not only by concerns of planetary damage and economics but also a desire to conserve more and waste less as a point of basic societal betterment. Solar energy is commonly acknowledged as a promising renewable energy source to support the future of humanity [1, 2]. To date, besides the conventional silicon solar cells (single crystal and mesoporous) and thin film solar cells, several new photovoltaic technologies for converting solar photons into electricity have been developed. These include organic photovoltaic cells (OPVs), dye-sensitized solar cells (DSSCs) and quantum dot-sensitized solar cells (QDSCs). Such devices have inspired much research interest due to their potential to serve as low-cost alternatives to the traditional solar cell modules [3–7].

Recently, a new type of solar cell based on mixed organic-inorganic halide perovskites ABX_3 (Fig. 1.1a, A = CH_3NH_3 (MA) or NH_2CHNH_2 (FA), B = Pb or Sn, X = Cl, Br or I) has quickly attracted much attention and gradually become one of the most important all-solid-state solar cells materials in what are called perovskite solar cells (PSCs) [8–15]. As the core of PSCs, hybrid organic-inorganic halide perovskites ABX_3 possess some fascinating properties such as an appropriate band gap, a high absorption coefficient, a long charge diffusion length and solution processability. Taken together, this gives PSCs some of the highest efficiencies with values as large as 20 % [16]. Perovskite, named after the Russian mineralogist Lew A. Perovski, is defined as a class of compounds by the general formula ABX_3 in which X is an anion and A and B are cations of different sizes (where A > B) [17]. Ideally, a perovskite structure consists of corner sharing BX_6 octahedra with the A ion placed in the cuboctahedral interstices which belong to the cubic $Pm\bar{3}m$ crystal structure, as shown in Fig. 1.1a [18]. In the hybrid organometal halide perovskites, A is an organic cation (i.e., MA^+ or FA^+), B is a metal cation (i.e., Sn^{2+} or Pb^{2+}), and X is a halide anion (i.e., Cl^-, Br^- or I^-) [19, 20]. In particular, hybrid organometal halide perovskites $ABX_{3-x}Y_x$ with mixed halides, for example, $MAPbI_{3-x}Cl_x$ and $MAPbI_{3-x}Br_x$ (Fig. 1.1b, c) have also attracted special attention due to their tunable optical properties which leads to improved performance in PSCs [21–23].

As indicated in Fig. 1.2, early in 2009, hybrid organometal halide perovskites were initially used in conventional liquid electrolyte-based DSSCs as light absorbers, yielding PCEs of 3.13 % ($MAPbBr_3$) and 3.81 % ($MAPbI_3$), respectively [24]. In 2011, Park and coworkers achieved a PCE of 6.54 % in a perovskite quantum dot-sensitized 3.6 μm-thick TiO_2 film using the iodide/iodine redox couple [25]. However, these solar cells are usually unstable and the performance degraded rapidly due to the dissolution or decomposition of perovskites in the liquid electrolyte.

The real breakthrough for PSCs came in 2012, as shown in Fig. 1.2 and Table 1.1, when Grätzel's group employed a solid hole-transporting material (HTM) 2,2',7,7'-tetrakis(N,N-di-p-methoxyphenylamine)-9,9'-spirobifluorene (spiro-MeOTAD) instead of the conventional liquid redox electrolyte. In their PSCs, PCEs of 9.7 % were achieved under AM 1.5 G illumination along with excellent long term stability for over 500 h. Charge separation proceeded via electron transfer to a sub-micron-thick mesoporous TiO_2 film and hole injection from the excited $MAPbI_3$ into

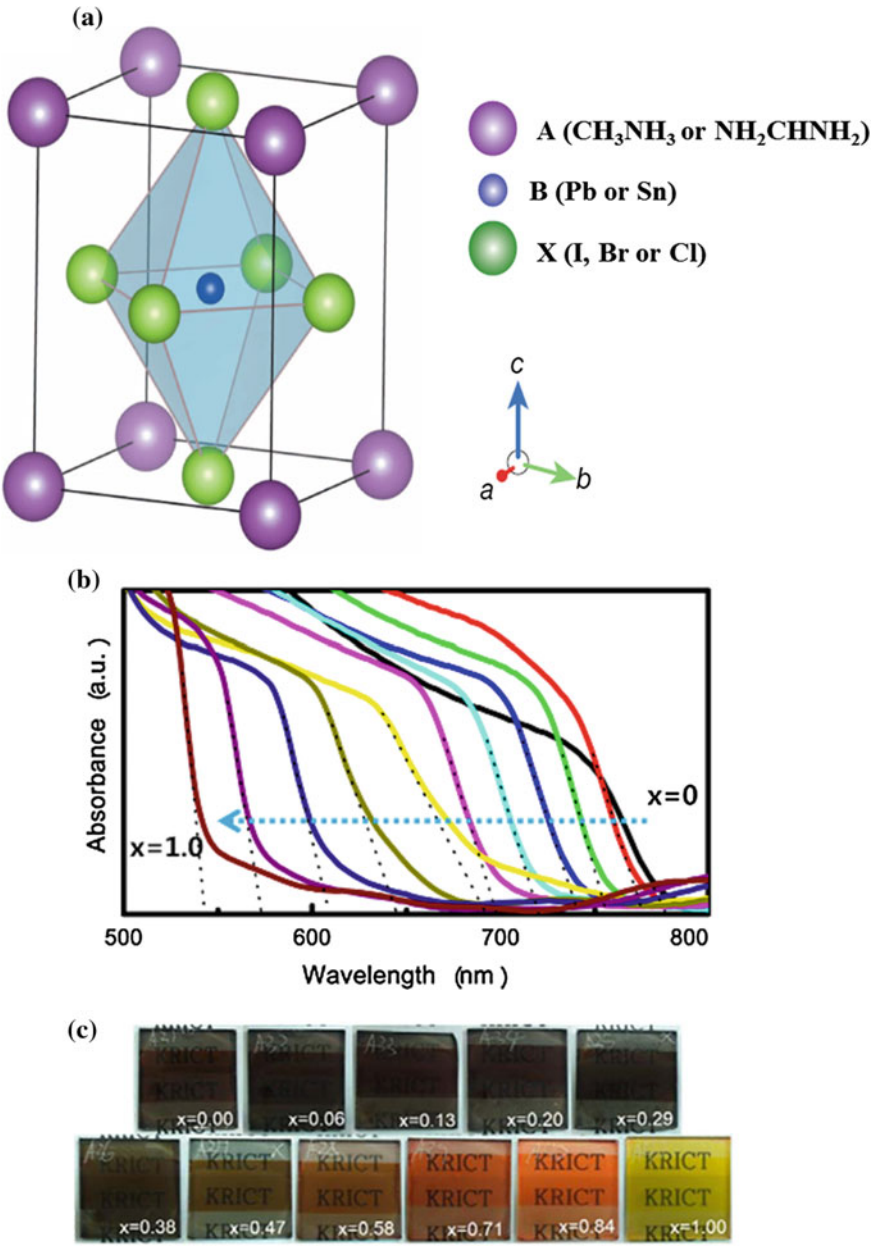

Fig. 1.1 **a** Crystal structure of ABX_3, **b** UV-vis absorption spectra and **c** photographs of $MAPbI_{3-x}Br_x$ (reprinted with permission from [18] **a** M. Liu et al., Nature 2013, 501, 395–398. [21] **b–c** J.H. Noh et al., Nano Lett. 2013, 13, 1764–1769. Copyright © Nature Publishing Group and American Chemical Society)

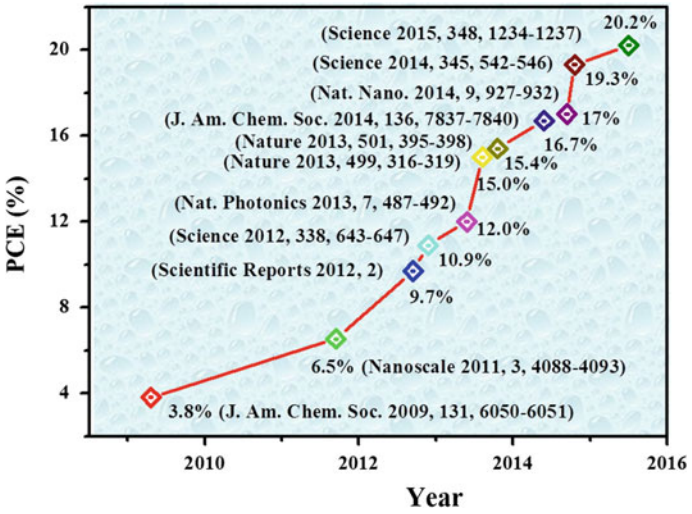

Fig. 1.2 Progress in perovskite solar cells demonstrating the amazingly sharp rise in PCE over the past 6 years

Table 1.1 Photovoltaic performance of PSCs depending on materials and cell configurations

Cell configuration[e]	J_{sc} (mA/cm^2)[a]	V_{oc} (V)[b]	FF[c]	PCE (%)[d]	References
FTO/bl-TiO_2/mp-TiO_2/$MAPbI_3$/ Spiro-MeOTAD/Au	17.6	0.888	0.62	9.7	[26]
FTO/bl-TiO_2/mp-Al_2O_3/ $MAPbI_2Cl$/Spiro-MeOTAD/Ag	17.8	0.98	0.63	10.9	[27]
FTO/bl-TiO_2/mp-TiO_2/$MAPbI_3$/PTAA/Au	16.5	0.997	0.727	12.0	[28]
FTO/bl-TiO_2/mp-Al_2O_3/$MAPbI_{3-x}Br_x$/ PTAA/Ag	18.0	1.02	0.67	12.3	[29]
FTO/bl-TiO_2/mp-TiO_2/$MAPbI_3$/ spiro-MeOTAD/Au	20.0	0.993	0.73	15.0	[30]
FTO/bl-TiO_2/$MAPbI_{3-x}Cl_x$/ spiro-MeOTAD/Ag	21.5	1.07	0.67	15.4	[18]
FTO/bl-TiO_2/mp-TiO_2/$MAPbI_3$/PTAA/Au	21.3	1.04	0.73	16.2	[31]
FTO/bl-TiO_2/mp-TiO_2/$MAPbI_3$/ pp-spiro-MeOTAD/Au	21.2	1.02	0.776	16.7	[32]
FTO/bl-TiO_2/mp-TiO_2/$MAPbI_3$ cuboid/spiro-MeOTAD/Au	21.64	1.056	0.741	17.01	[33]
ITO-PEIT/bl-Y doped-TiO_2/M $APbI_{3-x}Cl_x$/spiro-MeOTAD/Au	22.75	1.13	0.75	19.3	[34]
FTO/bl-TiO_2/mp-TiO_2/$FAPbI_3$/PTAA/Au	24.7	1.06	0.775	20.2	[35]

[a]Short-circuit voltage
[b]Open-circuit voltage
[c]Fill factor
[d]Power conversion efficiency
[e]*bl* stands for blocking layer and *mp* stands for mesoporous

the spiro-MeOTAD [26]. Almost simultaneously in 2012 (Fig. 1.2 and Table 1.1), Snaith et al. replaced the *n*-type mesoporous TiO_2 with insulating mesoporous Al_2O_3 in PSCs. The FTO/blocking layer (bl)-TiO_2/mesoporous (mp)-Al_2O_3/$MAPbI_2Cl$/spiro-MeOTAD/Ag-based device, termed the meso-superstructured solar cell (MSSC), boosted the reported PCEs to 10.9 %. Moreover, it was also revealed that perovskites can be used not only as sensitizers but also as an electron and hole transport layer between cell terminals [27].

In early 2013 (Fig. 1.2 and Table 1.1), a further jump to a PCE of 12.0 % was obtained by Seok, Grätzel et al. by using a bicontinuous three-dimensional nanocomposite of mp-TiO_2 with $MAPbI_3$ perovskites as a light harvester and poly-triarylamine (PTAA) as a hole transport material (HTM) [28]. Subsequently, Seok et al. further improved the PCE to 12.3 % using similar structures but with mixed-halide $MAPbI_{3-x}Br_x$ perovskites [29]. In late 2013 (Fig. 1.2 and Table 1.1), further progress was reported by two research groups with PCEs above 15 % [18, 30]. First, Grätzel et al. developed a sequential deposition process to fabricate $MAPbI_3$ films with improved morphology on the TiO_2 scaffold layers and measured a remarkable PCE of 15 % in a FTO/bl-TiO_2/mp-TiO_2/$MAPbI_3$/spiro-MeOTAD/Au-based PSC [30]. Subsequently, Snaith et al. deposited a high quality $MAPbI_{3-x}Cl_x$ film via two-source thermal evaporation in a new planar heterojunction (PHJ) perovskite solar cell (FTO/bl-TiO_2/$MAPbI_{3-x}Cl_x$/spiro-MeOTAD/Ag) without the mp-TiO_2 scaffold and achieved a PCE of 15.4 % [18].

In early 2014 (Fig. 1.2 and Table 1.1), Seok et al. further improved the PCEs of FTO/bl-TiO_2/mp-TiO_2/$MAPbI_3$/PTAA/Au-based PSCs to 16.2 % [31]. At the same time, Lee and Seok achieved a 16.7 % PCE in PSCs with a similar solar cell structure by instead using spiro-MeOTAD derivatives as the HTM [32]. Later, Park and Grätzel applied a two-step spin coating procedure to control the size of the $MAPbI_3$ cuboids during their growth and achieved a PCE of 17.01 % [33]. This was increased to a confirmed efficiency of 17.9 % in early 2014 by Seok [8]. Then, Yang et al. further raised the PCE to 19.3 % in a planar geometry by using an ITO-PEIT/bl-Yttruim doped-TiO_2/$MAPbI_{3-x}Cl_x$/spiro-MeOTAD/Au device structure [34]. In 2015, Seok et al. fabricated $FAPbI_3$-based PSCs with the highest PCE to date (up to 20.2 %) using a FTO-glass/bl-TiO_2/mp-TiO_2/$FAPbI_3$/PTAA/Au cell structure [35].

During the past few years, extensive investigation into the morphology and crystal optimization of perovskites [36–44], the material selection and deposition modulation of blocking and scaffold layers [33, 45–48], HTM modification and interface/band-gap engineering [28, 49–54] has led to an accelerated boost in the reported device PCEs from less than 4 % to over 20 %. This trend has opened up a new way to develop highly efficient solid-state solar cells at low cost and high stability.

The cell configuration of PSCs can be generally classified into two types: porous and planar architectures [55]. As shown in Fig. 1.3, three cell models can be found in the porous configuration [56, 57]: (1) sensitization: the perovskite with nanodot morphology is produced in one step by spin-coating onto the mp-TiO_2 surface where the amount of deposited perovskite is relatively low and the HTM is

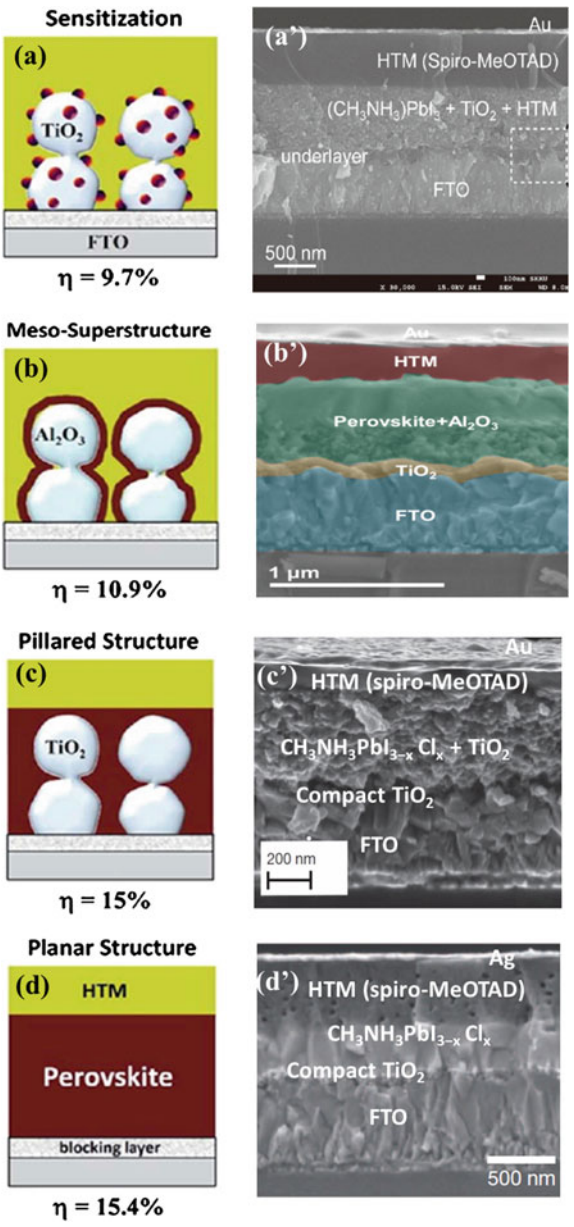

Fig. 1.3 The evolution of device structures for perovskite solar cells: **a**–**d** schematic diagrams, and **a′**–**d′** cross-sectional SEM images of different cell modules (reprinted with permission from [56] **a**–**d** H.-S. Kim et al., J. Phys. Chem. C 2014, 118, 5615–5625. [26] **a′** H.-S. Kim et al., Scientific Reports 2012, 2. [150] **b′** S. Guarnera et al., J. Phys. Chem. Lett. 2015, 6, 432–437. [30] **c′** J. Burschka et al., Nature 2013, 499, 316–320. [18] **d′** M. Liu et al., Nature 2013, 501, 395–398. Copyright © Nature Publishing Group and American Chemical Society)

infiltrated into the mp-TiO_2 pores [26]; (2) meso-superstructure: a thin perovskite layer is loaded on the mp-Al_2O_3 surface and the HTM is infiltrated into the mp-Al_2O_3 pores [27]; (3) pillared structure: the mp-TiO_2 pores are filled with perovskite instead of HTM and a thin capping layer (over layer) of perovskite is deposited to contact the HTM [30].

In the planar configuration, a mesoporous oxide film is not necessary because perovskite is capable of transporting electrons and holes. However, a thin blocking layer is still required to prevent direct contact between the conductive substrate and the HTM [58]. It is worth noting that the mesoporous scaffold layers can not only be composed of semiconductor materials (e.g. TiO_2, ZnO, NiO, SnO_2, WO_3, metal sulfides) [59–64], but also can contain metal oxide insulators (e.g. Al_2O_3, ZrO_2, SiO_2) owing to the ability of perovskites to transport electrons as well as holes [65–67]. In the following section, a comprehensive summary of the performance of such metal oxide semiconductors and insulators, as well as other materials (e.g., carbon materials) used in PSCs, is presented.

1.2 Nanostructured Scaffold Layers in PSCs

For nanostructured scaffolds, significant progress in the deposition technology, material type, film morphology, and layer thickness has been made as a consequence of the rapid development of PSCs in order to accommodate a variety of device architectures [47, 68–72]. In the following section, some representative examples will be presented and discussed.

1.2.1 Nanostructured TiO_2 Layers

It has been observed that the morphology, thickness and crystallinity of the TiO_2 electron-blocking layer and mesostructured layer play a crucial role in the efficiency of PSCs [73–75]. Next, a general overview and some detailed description are presented on the recent development of nanostructured TiO_2 as applied in PSCs.

1.2.1.1 Compact TiO_2 Blocking Layers

For typical porous and planar PSCs, the fabrication processes starts with the deposition of a compact TiO_2 layer onto a pre-cleaned conductive substrate which acts as a blocking layer to prevent direct contact between the conductive substrate and the infiltrated HTM layer [18, 26]. At present, four strategies have been developed to deposited such a compact TiO_2 layer [76], including (1) spin-coating a colloidal dispersion of TiO_2 nanoparticles (NPs) followed by a thermal treatment (titanium source: $TiCl_4$ [77], titanium tetraisopropoxide (TTIP) [78], and tetra-*n*-butyl-titanate [79]); (2) spin-coating the titanium precursor solutions followed by a thermal treatment (titanium source: TTIP [80], tetra-*n*-butyl-titanate [81, 82], and titanium diisopropoxidebis(acetylacetonate) [33]); (3) spray pyrolysis deposition (titanium source: TTIP [83], titanium diisopropoxidebis(acetylacetonate) [33, 84]); (4) atomic layer deposition (ALD) (titanium source: $TiCl_4$ [85], cyclopentadienyl alkylamido

titanium [86], tetrakis(dimethylamino) titanium [87]). Other methods such as thermal oxidation of a sputtered Ti film [88] and magnetron sputtering TiO_2 NPs on FTO substrates [89, 90] have been reported as well. In particular, the ALD method enables the deposition of higher quality films, as defined by lower pinhole density, in the range of temperatures compatible with conductive plastic substrates [86].

For the fabrication of flexible PSCs, several solutions have been exploited to avoid the high temperature heating treatment: (1) low temperature methods (e.g., spin coating followed by low temperature annealing [77], ultrasonic spray coating [91], and dip-coating [92]) to prepare the TiO_2 compact layers without high temperature heating treatment; (2) TiO_2 layer deposition through RF magnetic sputtering as an efficient barrier layer to replace the TiO_2 compact layer and create a PET-ITO/Ti/$MAPbI_3$/spiro-MeOTAD/Ag based flexible PSC with a PCE of 8.39 % (Fig. 1.4a–c) [93]; and (3) Ti metal as the conductive substrate for flexible PSCs with a PCE of 6.15 % by using a silver thin film as a semi-transparent top electrode on the Ti substrate (Fig. 1.4d–f) [94].

Furthermore, in order to improve the electrical properties at the interface between the perovskite layer and the compact TiO_2 layer, surface modification techniques such as $TiCl_4$- and UV(O_3)-treatment were employed to increase the PCEs of planar PSCs from 13.7 to 16.3 and 16.9 %, respectively [95]. Also, thin dense Mg-doped TiO_2 was used as the blocking layer instead of pure TiO_2 because of its better properties including improved optical transmission properties, up shifted conduction band minimum (CBM) and downshifted valence band maximum (VBM), better hole-blocking effect, and higher electron lifetime. These properties led to enhanced performance (PCE: pure TiO_2-9.16 % vs. Mg-doped TiO_2-12.28 %) in porous PSCs [96].

1.2.1.2 Mesoporous TiO_2 Scaffold Layers

As the most common device configuration for PSCs, porous PSCs based on perovskite sensitized mesoporous TiO_2 scaffolds have achieved PCEs from 9.7 % to over 20 % [26, 35]. Mesoporous TiO_2 films not only transport photo-generated electrons from perovskite sensitizers but also assist in the perovskite crystal transformation when the perovskite layer is deposited by the sequential deposition process [76]. In general, a mesoporous TiO_2 layer is deposited by spin-coating, screen-printing or doctor blading the TiO_2 nanoparticle (NP) paste on the top of the compact TiO_2 blocking layer followed by a sintering process [97–101]. Importantly, efficient infiltration of the perovskite and the subsequent HTM into the pores of the mesoporous scaffold is necessary for high performance PSCs. For mesoporous TiO_2 scaffolds, several aspects have been investigated to study their effect on the porous PSC device performance.

First, Kim et al. showed that the increase of the TiO_2 film thickness reduced the open circuit voltage (V_{OC}) and fill factor (FF) of cell devices. This was attributed to an increase in dark current and electron transport resistance according to impedance spectroscopic studies (Fig. 1.5a–b). Meanwhile, the short circuit photocurrent

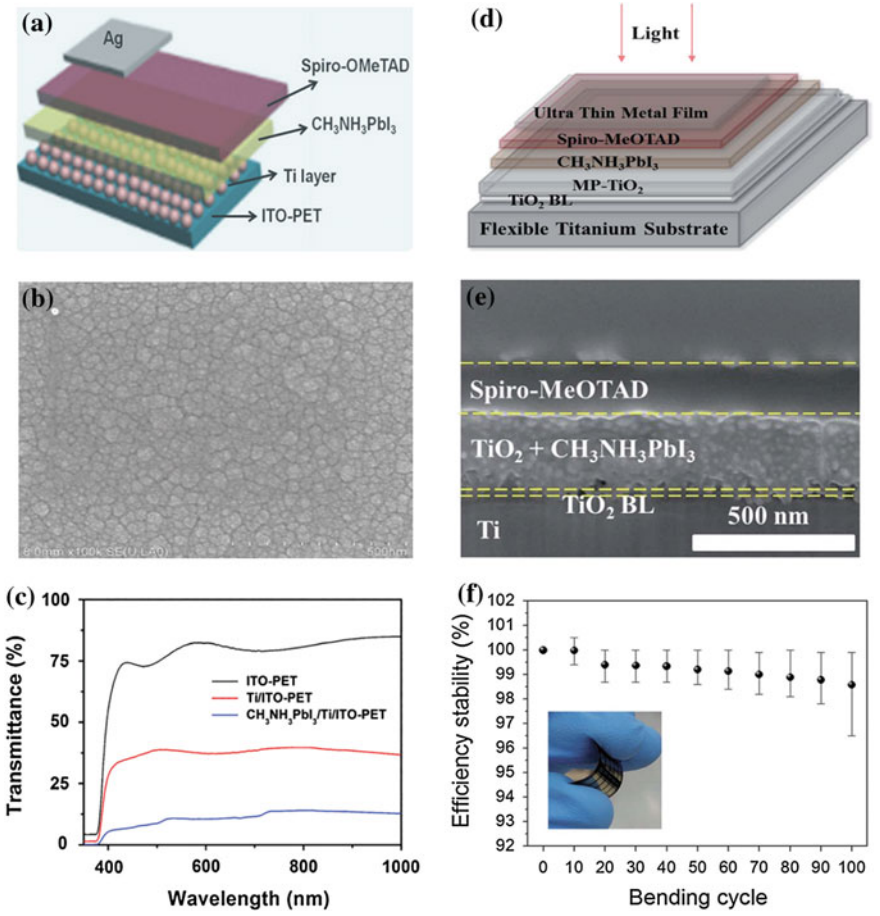

Fig. 1.4 **a** Schematic representation of the fabricated PET-ITO/Ti/$MAPbI_3$/spiro-MeOTAD/Ag flexible PSC, **b** SEM image of a Ti thin film with a thickness of ~100 nm, **c** UV-vis spectra of different samples, **d** device structure, **e** Cross-sectional image, and **f** efficiency stability as a function of bending cycle in a PSC using a Ti substrate with a semi-transparent Ag layer. Inset image is an optical image taken during a bending test (reprinted with permission from [93] **a**–**c** S. Ameen et al., Dalton Trans. 2015, 44, 6439–6448. [94] **d**–**f** M. Lee et al., J. Mater. Chem. A 2015, 3, 4129–4133. Copyright © The Royal Society of Chemistry)

density (J_{SC}) was not strongly influenced by a change in thickness of the TiO_2 layer from 0.6 to 1.4 μm; maintaining a high level of 16–17 mA cm^{-2} due to the large optical absorption [26]. Since the electron diffusion length in $MAPbI_3$ is about 100 nm [102], studies have revealed that when the thickness of mesoporous TiO_2 exceeds 600 nm, the electron/hole transport encounters larger resistances. This results in a significant loss of V_{OC} and therefore FF [103]. As a result, the optimized thickness for mesoporous TiO_2 should be controlled in the range of 400–600 nm [30, 104–107].

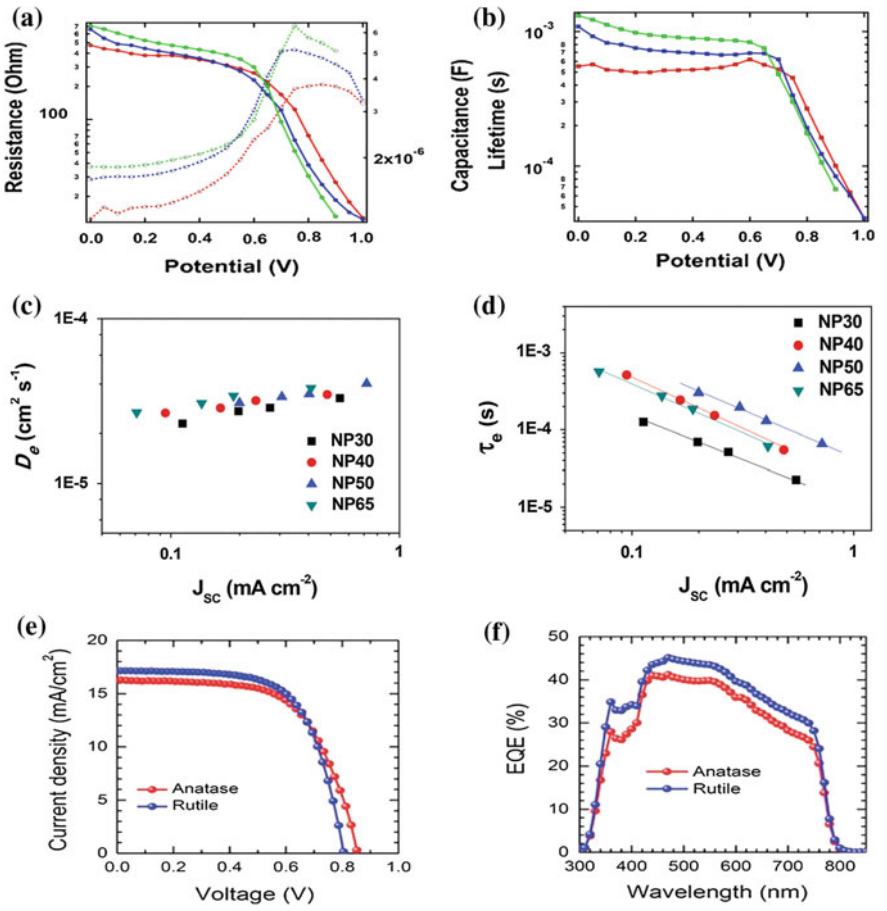

Fig. 1.5 **a** Recombination resistance (*solid lines*) and accompanying capacitance (*dashed lines*), and **b** electron lifetime under illumination of TiO_2, thickness: *red* 0.6 μm, *blue* 1.15 μm and *green* 1.4 μm. Plots of **c** the electron diffusion coefficient (D_e) versus J_{SC} and **d** the electron lifetime (τ_e) versus J_{SC} for the PSCs employing TiO_2 NPs with different sizes. **e** Current density-voltage (J-V) curves and **f** EQE spectra for the PSCs based on anatase (*red*) and rutile (*blue*) TiO_2 films (reprinted with permission from [26] **a**, **b** H.-S. Kim et al., Scientific Reports 2012, 2. [70] **c**, **d** S.D. Sung et al., Nanoscale 2015, 7, 8898–8906. [75] **e, f** J.-W. Lee et al., J. Mater. Chem. A 2014, 2, 9251–9259. Copyright © Nature Publishing Group and the Royal Society of Chemistry) (Color figure online)

Second, the size of TiO_2 NPs also impacts the device performance of PSCs. Han et al. used anatase TiO_2 scaffold layers with different particle sizes (15–30 nm) to investigate their performance in hole-conductor-free fully printable mesoscopic PSCs based on a carbon counter electrode and $(5\text{-AVA})_x(MA)_{1-x}PbI_3$ perovskite, and found that the size of TiO_2 particles not only affected the infiltration of the precursor and the contact between the perovskite crystal and TiO_2, but also

significantly influenced the charge transfer kinetics at the perovskite/TiO_2 interface. The device based on TiO_2 NPs with a diameter of 25 nm exhibited the best PCE of 13.41 % [108]. Meanwhile, Sung et al. prepared larger anatase TiO_2 NPs with diameter sizes from 30 to 65 nm and found that the spherical TiO_2 NP of 50 nm size exhibited the longest electron lifetime although the electron injection from perovskite to TiO_2 was less efficient than the devices with smaller TiO_2 NPs (Fig. 1.5c, d) and offered the highest PCE of 17.19 % (J_{SC}: 21.58 mA cm^{-2}, V_{OC}: 1049 mV, FF: 0.759) when it was employed in porous PSCs [70].

Finally, Yella, Grätzel et al. found that the nanocrystalline rutile TiO_2 prepared via hydrolysis of $TiCl_4$ at 70 °C achieved a much better performance (PCE: 13.7 %) than a planar TiO_2 (anatase) film (PCE: 3.7 %) prepared by high temperature spin coating of $TiCl_4$. This is likely attributed to the formation of an intimate junction of large interfacial area between the nanocrystalline rutile TiO_2 and the $MAPbI_3$ layer. This leads to effective extraction of the photo-generated electrons [62]. Similarly, Park et al. reported that the device performance of PSCs can be influenced by the crystal phase of TiO_2. In terms of infiltration of the $MAPbI_3$ perovskite and the smooth surface of the perovskite capping layer, the rutile TiO_2 film was found to be better than the anatase TiO_2 film. Rutile TiO_2-based devices (PCE: 14.46 %) exhibited better photovoltaic performance than the anatase TiO_2-based devices (PCE:13.99 %) along with lower standard deviation (Fig. 1.5e, f) [75].

1.2.1.3 One-Dimensional (1D) TiO_2 Scaffold Layers

Mesoscopic particle films as scaffolds in PSCs frequently suffer from complications such as inefficient electron transport in the nanocrystalline films and incomplete filling by organic HTMs in the mesopores of the films. Herein, one-dimensional (1D) nanostructures are considered as one promising alternative because they can provide a direct path for photo-generated electron transport. Moreover, the straight channels encountered in 1D architectures could benefit from the filling of the perovskites and the HTMs thus enhancing the hole transport efficiency [104, 109–111]. At present, several kinds of 1D nanostructures have been applied as scaffolds in PSCs including nanowires (NWs)/nanorods (NRs) [104, 109, 112–116], nanotubes (NTs) [110, 117], nanofibers (NFs) [111], and nanocones (NCs) [118].

In early 2013, Yang et al. organized PSC devices based on 1.5 μm-thick rutile TiO_2 NW arrays grown via a hydrothermal method, and obtained PCEs of 4.29 % and 4.87 % for $MAPbI_3$ and $MAPbI_2Br$ (Fig. 1.6a, b), respectively [113]. Subsequently, Park et al. raised the PCE to 9.4 % based on a sub-micrometer (~0.6 μm) rutile TiO_2 NR sensitized with $MAPbI_3$ perovskite nanodots (Fig. 1.6c, d) [112]. In 2014, Jiang et al. reported a PCE of 11.7 % for $MAPbI_3$ PSCs using optimized 900 nm-thick rutile TiO_2 NWs with an open face for effective material filling (Fig. 1.6e, f) [104]. Cai et al. synthesized rutile TiO_2 NR arrays on FTO substrates using an acid-free hydrothermal method in an aqueous Na_2EDTA solution with glycerol modified TTIP as the precursor. A PCE of 11.1 % was

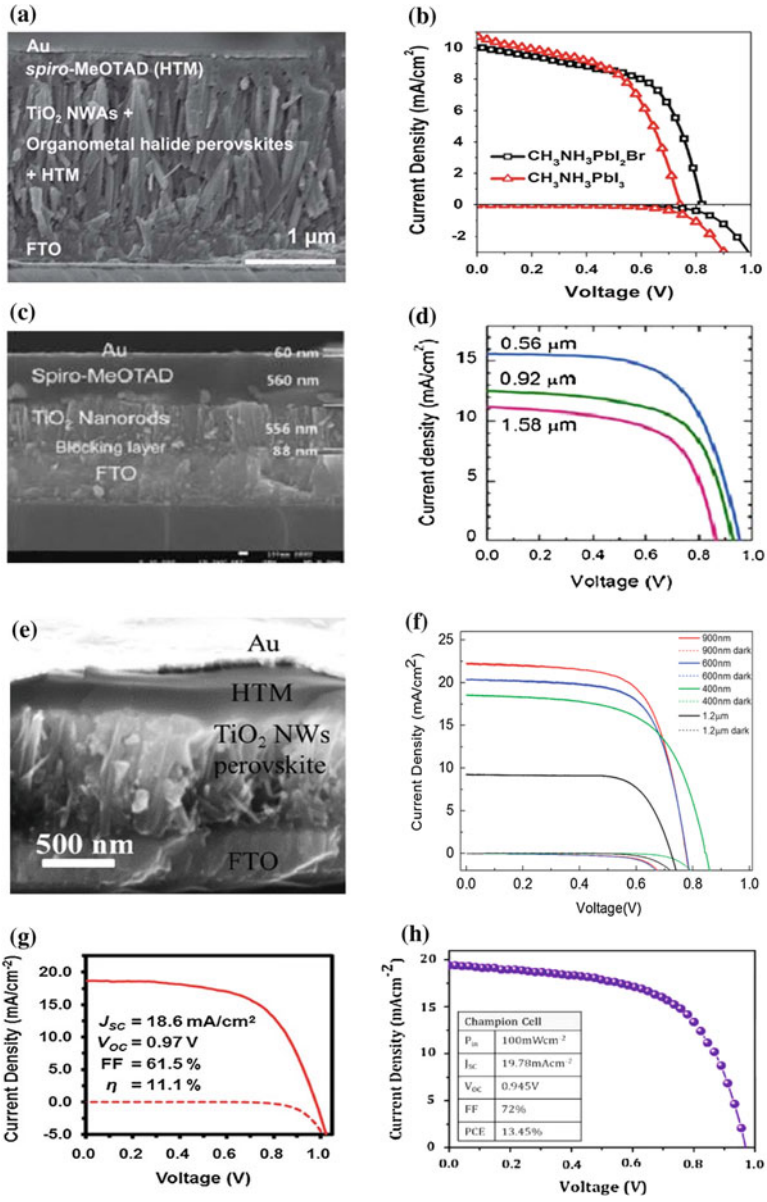

Fig. 1.6 **a**, **c**, **e** Cross-sectional SEM images and **b**, **d**, **f–h** J-V characteristics of the TiO_2 NW/NR-based PSCs (reprinted with permission from [113] **a, b** J. Qiu et al., Nanoscale 2013, 5, 3245–3248. [112] **c**, **d** H.-S. Kim et al., Nano Lett. 2013, 13, 2412–2417. [104] **e, f** Q. Jiang et al., Chem. Commun. 2014, 50, 14720–14723. [114] **g** B. Cai et al., J. Mater. Chem. C 2015, 3, 729–733. [116] **h** S.S. Mali et al., Chem. Mater. 2015, 27, 1541–1551. Copyright © The Royal Society of Chemistry and American Chemical Society)

obtained for the 0.7 μm-thick NR-based $MAPbI_3$ PSCs (Fig. 1.6g) [114]. In 2015, Mali et al. deposited an ultrathin TiO_2 passivation layer on the hydrothermally-grown TiO_2 NRs via ALD and achieved a significantly enhanced PCE of 13.45 % (pure NRs: 5.03 %, Fig. 1.6h) [116].

For 1D TiO_2 NTs, several groups have reported their application in PSCs [110, 117, 119, 120]. In 2014, Gao et al. first applied them as scaffold materials in $MAPbI_3$ PSCs. They fabricated freestanding TiO_2 NT array films with varied thicknesses by a two-step anodization process. The NTs were subsequently detached them from the Ti substrate by in situ field-assisted chemical dissolution and then transferred to the bl-TiO_2 layer pre-covered FTO substrates followed by the deposition of perovskite, HTM and novel metal films. The NT-based devices demonstrated improved light absorption and a reduced charge recombination rate as compared with TiO_2 NP-based systems using the same thickness of 4.8 μm (Fig. 1.7a, c). A peak PCE of 6.52 % was achieved with an optimized thickness of 2.3 μm [110]. Subsequently, Wang et al. prepared flexible PSCs based on Ti foil/TiO_2 NTs in conjunction with transparent carbon nanotubes (CNTs). These materials are deposited on top of perovskite to function as a hole collector as well as transparent electrode for light illumination. Such devices exhibited a PCE of 8.31 % and showed little deterioration after 100 mechanical bending cycles. This durability suggests potential applications in building wearable photovoltaic devices [117].

In addition, Dharani et al. employed electrospun TiO_2 NFs as scaffolds for PSCs yielding a PCE of 9.8 % (11.79 % at 0.1 sun). The open and porous nature of the electrospun NF network, which varied with the film thicknesses and fiber diameters, determined the device performance (Fig. 1.7d–f) [111]. Moreover, nanocone (NC) nanostructures were constructed under a nearly neutral hydrothermal process by using Na_2ETAD. A PCE of 11.9 % was achieved for such TiO_2 NC-based PSC devices. It was further found that electron transfer from $MAPbI_3$ to TiO_2 NCs was significantly faster than to TiO_2 NRs. This is an important factor to suppress charge recombination and improve device performance [118].

1.2.1.4 Two-Dimensional (2D) TiO2 Scaffold Layers

2D TiO_2 nanostructures have been widely used in DSSCs, and many studies have proved that the (001) facets of anatase TiO_2 are more reactive than the (101) facets, and it was proposed that the higher ionic charge of the exposed (001) facets strengthens the attachment of the light absorbers to the TiO_2 surface, thereby facilitating the electron injection into the conduction band of the oxide [121–123]. In 2014, Han et al. employed a double layer of TiO_2 NSs containing high levels of exposed (001) facets and ZrO_2 as a scaffold in a hole-conductor-free fully printable porous PSC (Fig. 1.8a). The high reactivity of (001) facets in TiO_2 NSs improved the interfacial properties between the perovskite and the electron collector (Fig. 1.8b, c). As a result, the PCE of this HTM-free PSC reached 10.64 % [124]. Subsequently, Dar et al. developed a TiO_2 scaffold composed of (001)-oriented nanoplatelets of anatase TiO_2 for PSCs (Fig. 1.8d, e). By adjusting

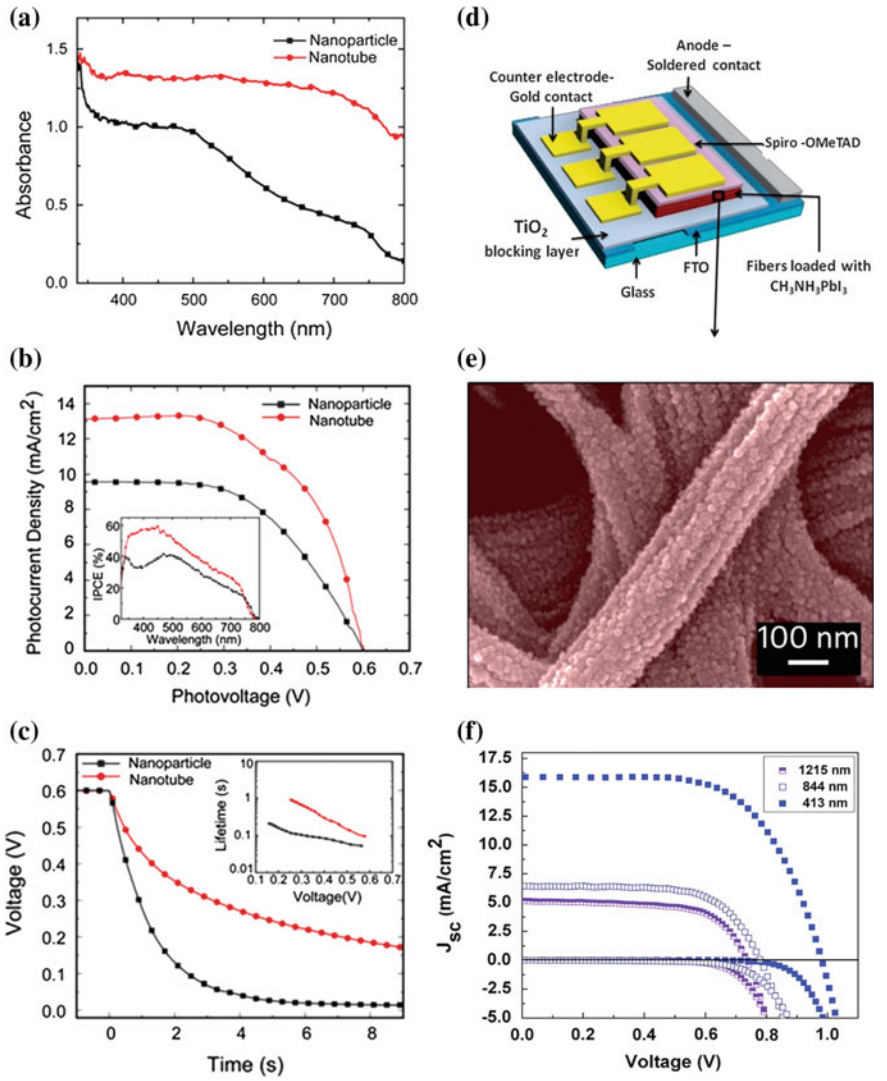

Fig. 1.7 **a** UV-Vis absorption of $MAPbI_3$ sensitized TiO_2 NP and NT electrodes, **b** J-V curves, IPCE (*Inset* of image b), and **c** open-circuit voltage decay and electron lifetimes (*Inset* of image c) of the PSCs with TiO_2 NP and NT electrodes. **d** Schematic illustration of the TiO_2 NF-based PSCs, **e** SEM of the $TiCl_4$ treated rough TiO_2 nanofibers, and **f** J-V curves of the PSCs based on TiO_2 NFs with different thicknesses (reprinted with permission from [110] **a–c** X. Gao et al., Chem. Commun. 2014, 50, 6368–6371. [111] **d**, **e** S. Dharani et al., Nanoscale 2014, 6, 1675–1679. Copyright © The Royal Society of Chemistry)

the thickness of the TiO_2 nanoplatelet and $MAPbI_3$/HTM layers, a PCE of 12.30 % was realized in the device using 100 nm-thick TiO_2 nanoplatelets and 300 nm-thick $MAPbI_3$/HTM layers (Fig. 1.8f) [125].

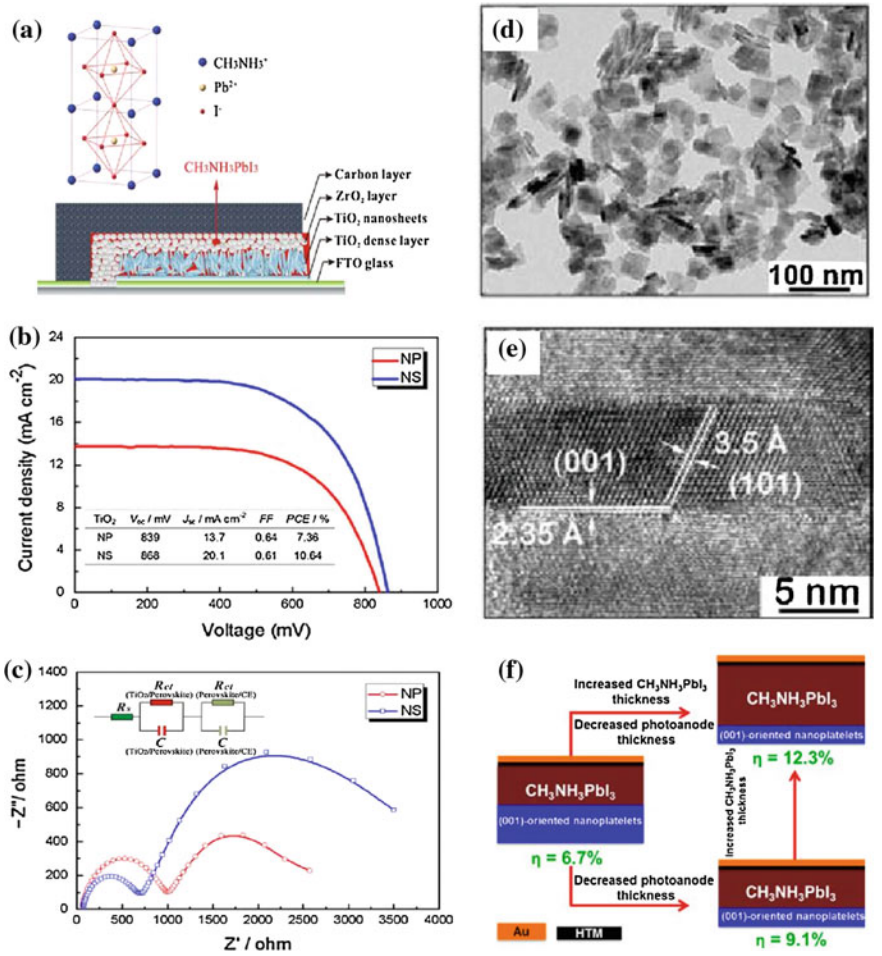

Fig. 1.8 **a** Schematic diagram, **b** J-V curves, and **c** Nyquist plots of a hole-conductor-free mesoscopic TiO_2/$MAPbI_3$ heterojunction solar cell based on P25 NPs/anatase TiO_2 NSs and carbon counter electrodes. **d** TEM and **e** HRTEM images for (001) anatase TiO_2 nanoplatelets. **f** Sketch map of the thickness optimization of the TiO_2 nanoplatelet-based PSCs (reprinted with permission from [124] **a**–**c** Y. Rong et al., J. Phys. Chem. Lett. 2014, 5, 2160–2164. [125] **d**–**f** M.I. Dar, et al., Chem. Mater. 2014, 26, 4675–4678. Copyright © American Chemical Society)

1.2.1.5 Three-Dimensional (3D) TiO_2 Scaffold Layers

Besides the above-mentioned nanostructures, some complicated 3D TiO_2 materials have been used in PSCs owing to their special properties such as high-speed conduction pathways and large surface areas for sufficient chemical reaction and/or dye loading [126–129]. For example, Kim, Park et al. made TiO_2 NRs into well-aligned helical arrays by the oblique-angle electron beam evaporation method

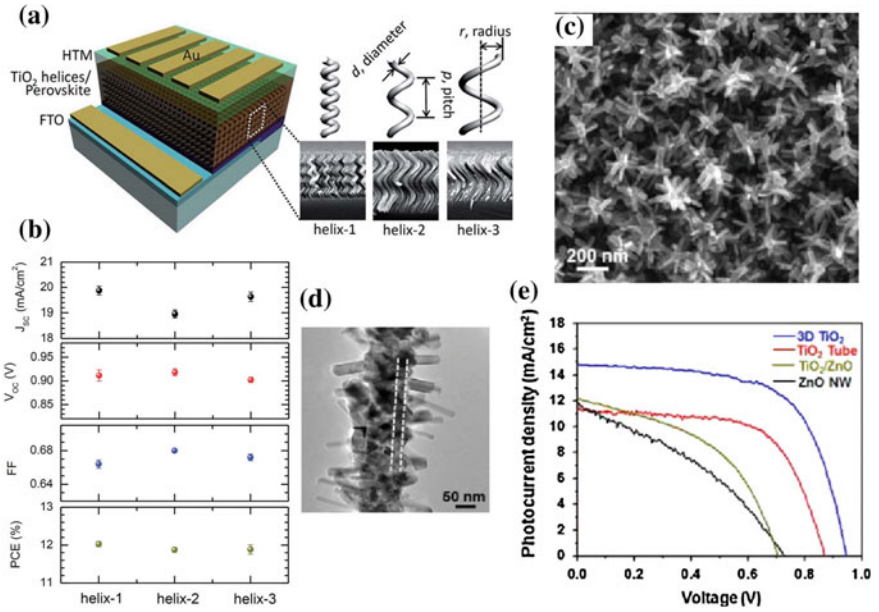

Fig. 1.9 **a** Schematic description of the PSC consisting of TiO_2 helices, and cross-sectional SEM images of three different TiO_2 helices grown on a silicon wafer. **b** Device performance of the TiO_2 helix-based PSCs. **c** *Top view* SEM, and **d** TEM images of the 3D TiO_2 NW architecture. **e** J-V curves of PSCs made from 3D TiO_2 nanostructures, TiO_2 NTs, TiO_2-coated ZnO NWs, and ZnO NWs with an identical film thickness of ~600 nm (reprinted with permission from [126] **a**, **b** J.-W. Lee et al., J. Mater. Chem. A 2015, 3, 9179–9186. [130] **c**–**e** Y. Yu et al., ACS Nano 2015, 9, 564–572. Copyright © The Royal Society of Chemistry and American Chemical Society)

(Fig. 1.9a). When this helical scaffold was used in PSCs, a best PCE of 12.03 % was measured (Fig. 1.9b). It was found that the contact area between TiO_2 and perovskite was critical to achieve a high performance PSC [126]. In particular, 3D hyper-branched NW/NR/NF architectures with high charge transport rates, sufficient surface area, and a 3D interconnected network for electron extraction were intensively studied and applied in solar cells. Yu et al. reported a 3D TiO_2 NW-based PSC with a 3D hierarchical TiO_2 architecture possessing a mixed anatase and rutile phases was constructed via a surface-reaction-limited pulsed chemical vapor deposition (SPCVD) technique (Fig. 1.9c, d). The highest PCE measured from such a device was 9.0 % (Fig. 3.9e). This was substantially higher than the PSCs made from ZnO NWs (PCE: 3.0 %), TiO_2-coated ZnO NWs (PCE: 4.0 %), and TiO_2 NTs (PCE: 6.2 %) [130].

Similarly, highly branched anatase TiO_2 NWs with varied orientation were grown via a facile one-step hydrothermal process on a FTO substrate. The multi-functionality of this dendritic TiO_2 thin film was found in PSCs: (1) its dense surface coverage on the transparent conductive oxide (TCO) substrate made it an effective electron transport layer; (2) its porosity enabled good perovskite anchoring

and TiO_2/perovskite interconnection; (3) its 3D configuration can efficiently capture and confine the incident light to yield improved light harvesting efficiency and electron transfer from the perovskite layer; and (4) the TiO_2 film can function as a good hole-blocking layer due to the varied orientation of the wires that would effectively block the direct contact between spiro-MeOTAD and FTO or between the back electrode and FTO even in the absence of a TiO_2 blocking layer. Consequently, the cell device achieved a high PCE of 14.21 % [127]. Moreover, Mahmood et al. introduced a 3D hyper-branched anatase TiO_2 NR-NF array prepared via a combination of electrospinning and hydrothermal processes. The hyper-branched scaffold with optimal electron transport and carrier lifetime led to highly efficient mesostructured PSCs with an average PCE of 15.03 % and a maximum PCE of 15.50 % [129].

1.2.1.6 Modified TiO_2 Scaffold Layers

A lot of work suggests that the interface between TiO_2 and $MAPbX_3$ is a crucial factor in determining the crystal growth of perovskite and the effectiveness of charge separation in devices. The interfacial treatment and modification of TiO_2 to adjust the electronic structure have been widely investigated to enhance the charge injection and collection and simultaneously reduce the carrier recombination in PSCs [34, 131–135]. Roughly, the strategies used to modify the TiO_2 scaffolds can be divided into three directions as follows.

(1) Surface treatment has frequently been used to improve the quality at the interface. A common approach is to introduce a carboxylate monolayer on the mesoporous TiO_2 surfaces to passivate the interface and then suppress the charge recombination in the solar cells (Fig. 1.10a–c) [136]. Another process involves chemical etching to tailor the inner space of TiO_2 electrodes in order to provide an optimized space for perovskite sensitizers and infiltration of a hole transport layer without sacrificing their original electron transport ability [137].

(2) Elemental doping has also been employed. Typical elements used include Y [34, 138, 139], Zr [140], Al [131], Sn [141], Nb [132], and Mg [142] among others. Yttrium was poorly soluble in TiO_2 and the segregation of Y_2O_3 at the TiO_2 surface facilitated an increased perovskite loading on TiO_2 (Fig. 1.10d, e) [138]. The Y-TiO_2-based devices exhibited faster photocurrent decay (Fig. 1.10f) suggesting a more efficient carrier extraction in the Y-TiO_2 devices which probably resulted from the improved interface at the Y-TiO_2 layer. Moreover, the Y-TiO_2 devices exhibited a slight upward shift of the Fermi level in the Y-TiO_2 layer. This indicates an increased donor concentration in response to the enhanced conductivity [34].

(3) Incorporation of cooperative materials (e.g., graphene [107, 143], Sb_2S_3 [144], ZrO_2 [67, 145, 146], MgO [134, 147], WO_3 [135], and Au [133]). For example, MgO surface modification can reduce the perovskite degradation

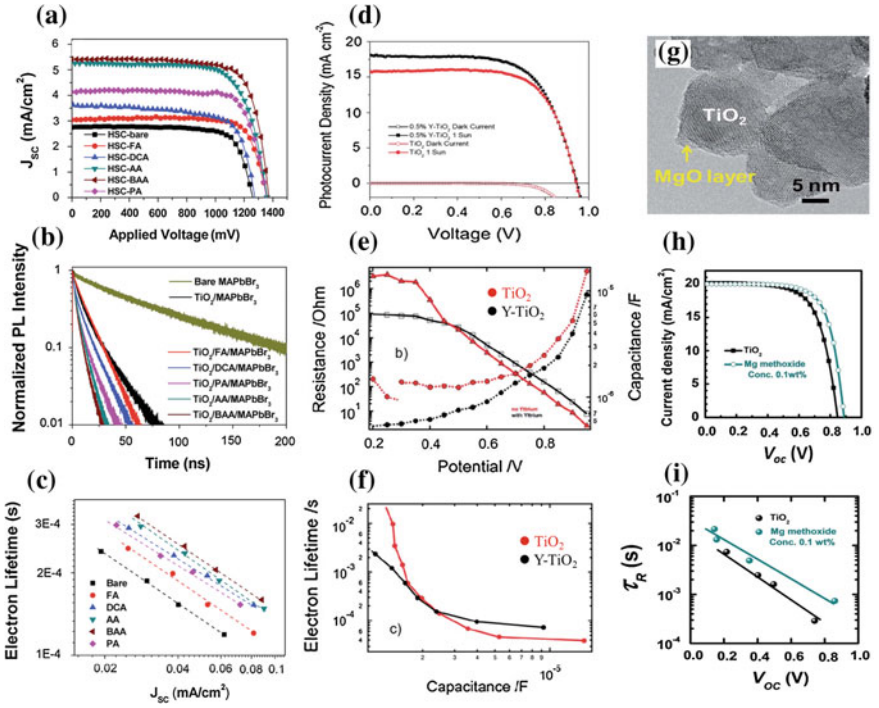

Fig. 1.10 **a** J-V curves, **b** PL decays, and **c** electron lifetime (τ_e) versus J_{SC} of PSCs employing different carboxylic acids. **d** J-V curves, **e** Recombination resistance (*solid lines*) and accompanying capacitance (*dashed lines*), and **f** evolution of the election lifetime as a function of capacitance of devices based on TiO_2 and Y-TiO_2. **g** HRTEM image of MgO/TiO_2 NPs. **h** J-V curves and (i) Electron lifetime of PSCs based on MgO/TiO_2 core-shell NPs and TiO_2 NPs (reprinted with permission from [136] **a–c** H.B. Kim et al., J. Mater. Chem. A 2015, 3, 9264–9270. [138] **d–f** P. Qin et al., Nanoscale 2014, 6, 1508–1514. [134] **g–i** G.S. Han et al., J. Mater. Chem. A 2015, 3, 9160–9164. Copyright © The Royal Society of Chemistry)

under H_2O and UV conditions by reducing the H_2O adsorbed on the mp-TiO_2 and blocking direct contact between TiO_2 and perovskite (Fig. 1.10g–j) [134, 147]. It also can reduce the electron/hole recombination at the TiO_2/$CH_3NH_3PbI_3$ surface thereby extending the carrier lifetime and yielding enhanced cell performance (Fig. 1.10k, l) [134, 147]. In addition, the PSC device incorporated with a unique sandwiched TiO_x-Au-NPs-TiO_x composite showed a 20–30 % performance enhancement. This was mainly attributed to the enhanced conductivity of the TiO_x layers to match the hole transporting capability, the decreased space-limited charges and the decreased surface potential of TiO_x film to lead to larger built-in potential in the device with improved V_{OC}. Both effects were ascribed to the plasmon-mediated hot carrier injection from the Au-NPs to TiO_x [133].

1.2.2 Nanostructured Al_2O_3 Layers

Since 2012 when Snaith et al. employed a mesoporous Al_2O_3 insulating layer as a scaffold in meso-superstructured PSC which gave a high PCE of 10.9 % and a high V_{OC} of 1.1 V [27], insulating Al_2O_3 materials have been extensively used in PSCs [36, 65, 68, 148–154]. Researchers find that the nature of the mesoporous scaffold impacts the final properties of perovskites and a high degree of preferential orientation has been detected for alumina scaffolds [155]. Furthermore, PSCs based on mesoporous Al_2O_3 electrodes present lower charge recombination rates than devices prepared on mesoporous TiO_2 [47].

It is worth noting that the PSCs based on the co-deposition of a combined Al_2O_3-perovskite layer, where the alumina NPs were suspended in the perovskite precursor solution and the Al_2O_3-perovskite layer was co-deposited by spin coating in a single deposition process followed by a low temperature heating step at T = 110 °C, showed an average PCE of 7.2 % on a non-sintered Al_2O_3 scaffold. [148] In addition, an ultrathin AlO_x layer was deposited onto a $MAPbI_3$ film using ALD, to construct a metal-insulator-semiconductor (MIS) back contact for the HTM-free PSC (Fig. 1.11a, b). This yielded a high PCE of 11.10 % after optimizing the ALD deposition cycles. It was revealed that this MIS back contact contributed to the enhancement in charge collection resulting from the electron blocking effect of the AlO_x layer (Fig. 1.11c) [154].

Moreover, when Al_2O_3 was coated on TiO_2 and $MAPbI_3$ layers, it could act as an insulating barrier to protect $MAPbI_3$ from degradation by moisture and suppress electron recombination between TiO_2 and spiro-MeOTAD. This leads to an enhancement of device stability when exposed to moisture [149, 150, 156]. In a similar study, an ultrathin Al_2O_3 film loaded on the HTM layer via an ALD method can act as a waterproofing agent to isolate the $MAPbI_3$ layers from moisture and thus realize enhanced device stability (Fig. 1.11d, e). Remarkably, the PCE of the PSC with ALD-Al_2O_3 retained ~90 % of its initial value after 24 days of storage in air (Fig. 1.11f) [68]. In addition, an insulating buffer layer between the perovskite and the metal was introduced into the PSC devices (Fig. 1.11g, h). This Al_2O_3 buffer layer significantly reduced the shunting degradation, inhibited the formation of a direct contact between the metal electrode and the perovskite, and improved the device stability with nearly no degradation in the first 350 h under simulated standard full sunlight (Fig. 1.11i). This Al_2O_3 buffer layer enabled the regulation of the thickness of the hole transporter layer which lead to lower device series resistance and higher PCEs [152].

1.2.3 Nanostructured ZnO Layers

Compared to TiO_2, ZnO is known to have a higher electron mobility which makes it an ideal choice for an electron-selective contact. Additionally, ZnO layers can be

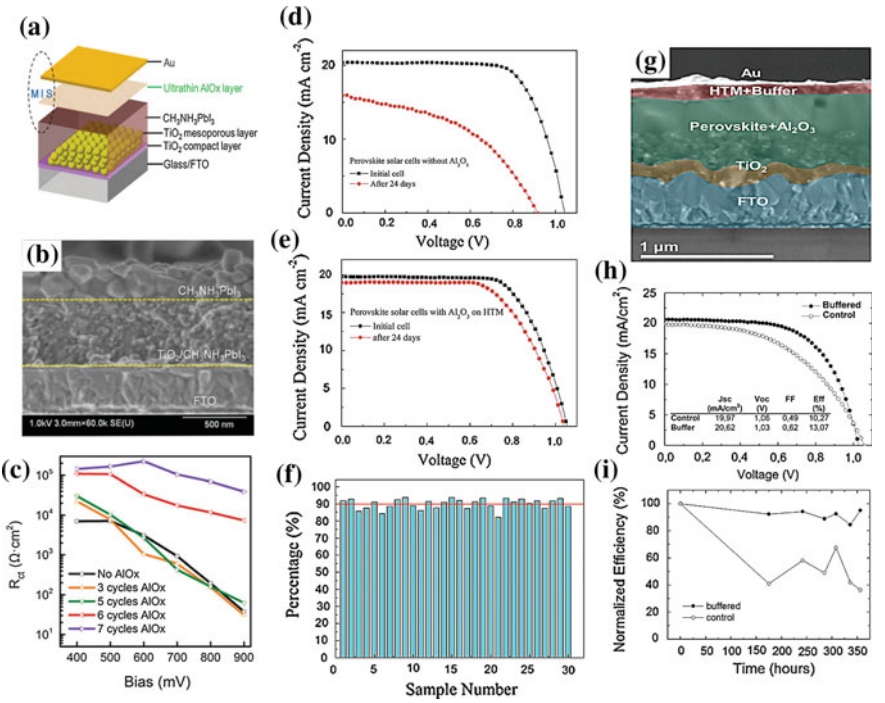

Fig. 1.11 **a** The scheme of the PSC with the MIS back contact, **b** cross-sectional SEM image of the FTO/TiO_2-$MAPbI_3$-AlO_x film, and **c** plots of charge transfer resistance (R_{ct}) for PSCs with different ALD cycles at various bias voltages. J-V characteristics for **d** FTO/bl-TiO_2/$MAPbI_3$/HTM/Ag and **e** FTO/bl-TiO_2/$MAPbI_3$/HTM/Al_2O_3/Ag at room temperature in 50 % humidity for 0 and 24 days. **f** The histogram of the PCE of thirty PSCs after 24 days in air compared with the original efficiency. **g** False color SEM image of a PSC with an Al_2O_3 buffer layer, **h** J-V curves and (i) normalized efficiency of the best solar cells realized with and without a buffer layer (reprinted with permission from [154] **a–c** H. Wei et al., Phys. Chem. Chem. Phys. 2015, 17, 4937–4944. [68] **d–f** X. Dong et al., J. Mater. Chem. A 2015, 3, 5360–5367. [152] **g–i** S. Guarnera et al., J. Phys. Chem. Lett. 2015, 6, 432–437. Copyright © The Royal Society of Chemistry and American Chemical Society)

easily deposited by spin coating and, depending on the use, require either no sintering step or merely a low-temperature heating treatment. This makes them ideal for the fabrication of flexible solar cells [157]. Devices based on ZnO NP scaffolds gave PCEs reaching 15.7 % [158], while ZnO-based flexible PSCs displayed PCEs over 13.14 % [157]. The solution-processing of the ZnO layers is simple, economical and proceeds at room temperature. This shows the remarkable advantages over TiO_2 scaffolds [64, 159, 160]. In addition to sol-gel methods [159], hydrothermal processes [161], chemical bath deposition [162], electrodeposition [64], and ALD methods [163] have also been used to grow ZnO structures for applications in PSCs. In addition to ZnO NP layers [164, 165], ZnO nanostructures in the form of NRs (Fig. 2.12a, b) [161, 162], NSs (Fig. 1.12c, d) [166] and quantum dots (Fig. 1.12e, f)

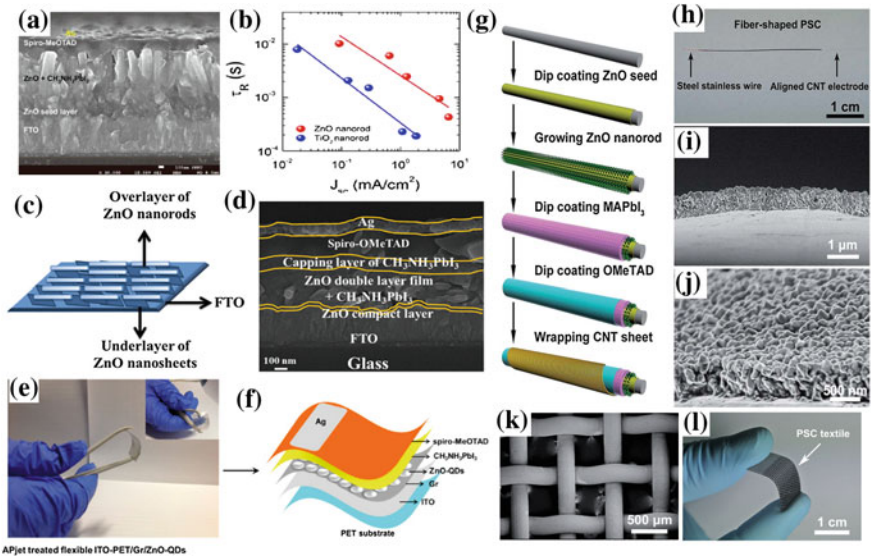

Fig. 1.12 **a** Cross-sectional SEM image of a ZnO NR-based PSC, **b** charge recombination τ_R as a function of light intensity, represented by photocurrent density, for the ZnO and TiO_2 nanorod-based PSCs. **c** Schematic illustration of ZnO film-based double-layer structure, and **d** cross-sectional SEM image of the corresponding PSC. **e** Photograph of ITO-PET/Graphene (Gr) and **f** schematic illustration of the flexible ZnO QD-based PSC. **g–j** Fiber-shaped PSC based on the aligned ZnO nano-obelisks: **g** Schematic illustration showing the fabrication process. **h** Photograph of a fiber-shaped PSC. SEM images of **i**, **j** a perovskite layer on the ZnO nano-obelisk array, and **k** the ZnO nano-obelisk array grown on a stainless steel fabric. **l** Photograph of the PSC fabric (reprinted with permission from [162] **a**, **b** D.Y. Son et al., J. Phys. Chem. C 2014, 118, 16567–16573. [166] **c**, **d** K. Mahmood et al., Nanoscale 2014, 6, 14674–14678. [167] **e**, **f** S. Ameen et al., J. Phys. Chem. C 2015, 119, 10379–10390. [173] **g–l** S. He et al., J. Mater. Chem. A 2015, 3, 9406–9410. Copyright © The Royal Society of Chemistry and American Chemical Society)

[167] have been used to fabricate PSC devices. Furthermore, doping treatments (e.g., Al, N and F) have been employed to modify the performance of ZnO nanostructures used in PSCs [168–171]. For large scale roll-to-roll production of flexible PSCs, a slot-die coating method was applied to realize the fabrication of fully printed ZnO-based PSCs yielding a peak PCE of 11.96 % [172]. Toward wearable solar cell device, PSCs in both fiber (Fig. 1.12g–j) and fabric (Fig. 1.12k, l) formats were built based on a ZnO nano-obelisk array, showing a peak PCE of 2.61 % [173].

1.2.4 Nanostructured NiO Layers

NiO is a cubic *p*-type semiconductor material with a large band gap that is widely applied in photovoltaic devices as a hole-conducting and collecting layer. When used

in PSCs, it has several advantages [174–176]: (1) NiO can prevent the degradation of PSC performance which is common in TiO_2-based PSCs because of the light induced desorption of surface-adsorbed oxygen on TiO_2 when it is subjected to long-term sunlight exposure; (2) unlike another p-type organic material, PEDOT:PSS (poly (3,4-ethylene dioxythiophene):poly(4-styrenesulfonate)), NiO is inert and does not corrode ITO substrates; (3) NiO_x has a tunable work function from 5.0 to 5.6 eV by using different O_2-plasma surface treatments. A better alignment of the work function of the NiO_x electrode interlayer with the VB (valence band) edge level of perovskite can be realized to improve the transfer of holes and increase the device photovoltage as well as other photovoltaic parameters; (4) NiO is suitable for the integration of PSC with silicon or copper indium gallium selenide (CIGS) solar cells to build tandem devices for higher device efficiency due to the inverse device architecture with holes flowing to the ITO substrate instead of the traditional device involving TiO_2 where electrons flow to the ITO substrate.

The NiO films used as hole-transporting layers (HTL) in PSCs have been prepared in various ways including spin coating of NiO precursors followed by annealing [174–176], sol-gel methods [177], RF sputtering [178, 179], screen-printing [180], spray pyrolysis [181], and pulsed laser deposition [60]. Both planar and mesoporous cell structures have been applied in NiO-based PSCs and their highest PCEs are 15.40 % [182] and 17.3 % [60], respectively. In addition, some special designs are also presented for NiO-based PSCs [182–185]. For example, Cu-doped NiO_x was used in planar PSCs based on a device configuration of ITO/Cu doped-NiO_x/$MAPbI_3$/[6,6]-phenyl-C_{61}-butyric acid methyl ester ($PC_{61}BM$)/C_{60}-bis surfactant/Ag. This device showed an impressive PCE up to 15.40 % and fair environmental stability [182]. A PSC device with a cell configuration of FTO/bl-TiO_2/mp-TiO_2/mp-NiO ($MAPbI_3$)/carbon achieved a PCE of 11.4 % by using NiO as an electron blocker and a hole conductor (Fig. 1.13a–c) [183]. An ultrathin NiO compact layer (10–20 nm) cooperating with an inert mesoporous Al_2O_3 (meso-Al_2O_3) scaffold was prepared in an inverted PSC with a cell configuration of FTO/NiO/meso-Al_2O_3/$MAPbI_3$/PCBM/bathocuproine(BCP)/Ag (Fig. 1.13d) and exhibited a PCE of 13.5 % owing to the minimal light absorption loss and interfacial recombination loss (Fig. 1.13e, f) [184].

1.2.5 Nanostructured Carbon Materials

Carbon materials are inexpensive and readily-available on an industrial scale. They are well-known, versatile and have been extensively applied in many fields [186, 187]. As to PSCs, carbon materials (e.g., grapheme, carbon, CNTs, and C_{60}) also play an important role and have been employed in almost all the functional layers [188–204].

For instance,

(1) Graphene: graphene nanoflakes were added into the electron collection layer of TiO_2 NPs in PSCs to reduce the device series resistance and recombination

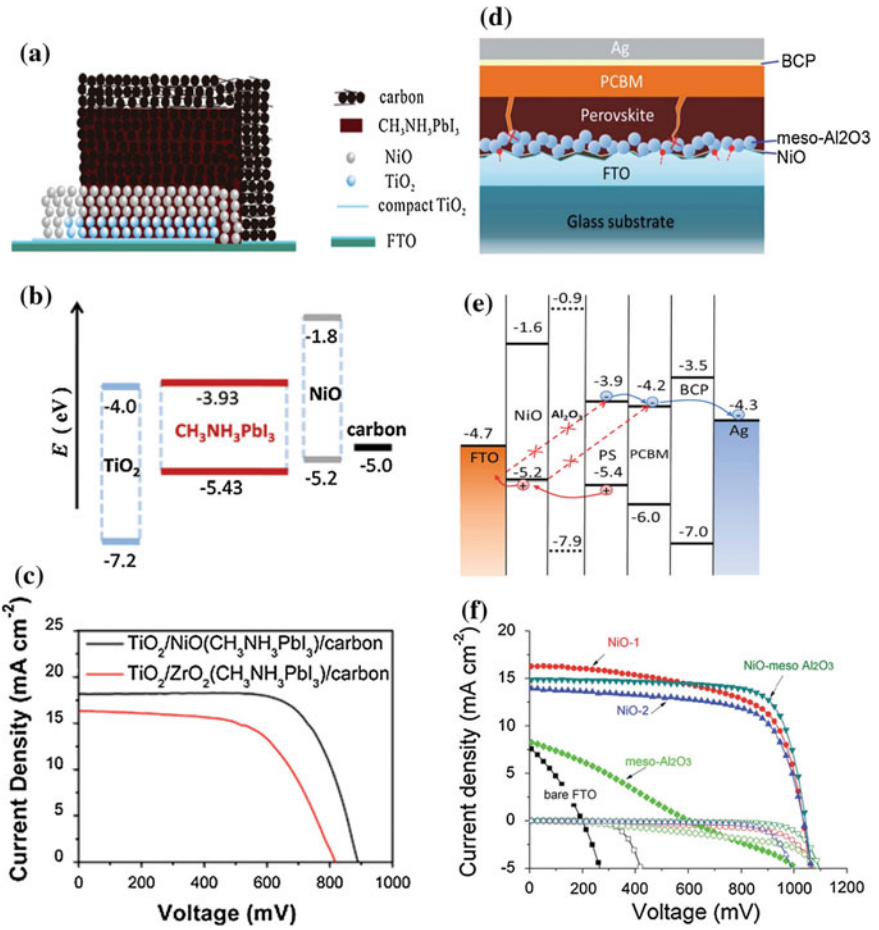

Fig. 1.13 **a**, **b** Cell configuration and energy level (versus vacuum) diagram of the TiO_2/NiO ($MAPbI_3$)/carbon device and **d**, **e** the inverted NiO/Al_2O_3-based PSCs. **c**, **f** J-V curves of the different PSCs (reprinted with permission from [183] **a–c** Z. Liu et al., Dalton Trans. 2015, 44, 3967–3973. [184] **d**, **e** W. Chen et al., *Energy Environ. Sci.* 2015, 8, 629–640. Copyright © The Royal Society of Chemistry)

losses (Fig. 1.14a, b) [143]; graphene quantum dots were inserted between the perovskite and the mesoporous TiO_2 to facilitate the electron transfer from the perovskite to the current collector (Fig. 1.14c, d) [107]; amphiphilic graphene oxide (GO) was used to form an insulating buffer layer between the perovskite and the HTL to prevent charge recombination [188]; GO and reduced graphene oxide (RGO) can act as hole conductors in inverted planar heterojunction PSCs (Fig. 1.14e, f) [189–191]; single-layered graphene (SG) and multilayered graphene (MG) function as hole extraction materials in PSCs with a device structure FTO/TiO_2/$MAPbI_3$/SG (or MG) [192]; multilayer

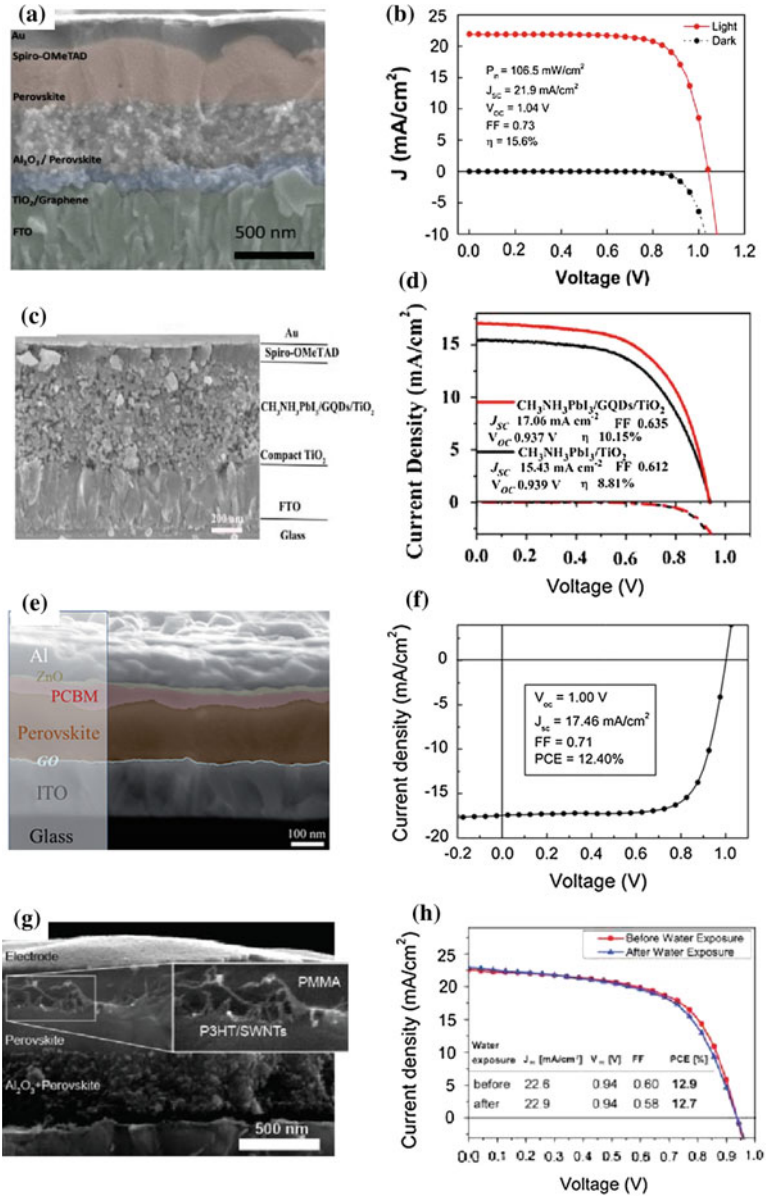

Fig. 1.14 Cross-sectional SEM images and I-V curves of the PSCs modified by **a–f** graphene materials and **g–h** carbon nanotubes (reprinted with permission from [143] **a, b**: J.T.-W. Wang et al., Nano Lett. 2014, 14, 724–730. [107] **c**, **d**: Z. Zhu et al., J. Am. Chem. Soc. 2014, 136, 3760–3763. [189] **e**, **f** Z. Wu et al., Nanoscale 2014, 6, 10505–10510. [202] **g**, **h** S.N. Habisreutinger et al., Nano Lett. 2014, 14, 5561–5568. Copyright © The Royal Society of Chemistry and American Chemical Society)

graphene prepared by CVD methods and modified by PEDOT:PSS was applied as a transparent top electrode on the HTL, which is promising for the fabrication of flexible PSCs by printing or roll-to-roll processes [193]; Graphene sheets were mixed into a functionalized nanographene (perthiolated trisulfur-annulated hexa-peri-hexabenzocoronene, TSHBC) which was employed as a HTM in PSCs [194].

(2) Carbon: carbon is typically used as the counter electrode in PSCs, especially in a hole-conductor-free cell configuration, by a low cost and fully-printable process [195–198]. Han's group developed a hole-conductor-free, fully printable mesoscopic PSC with carbon black counter electrodes (Fig. 2.8a) [67, 124, 197, 199, 200]. The resulting device gave a PCE of 12.8 % and a high environmental stability (>1000 h) in ambient air under full sunlight [200].

(3) Carbon nanotubes (CNTs): CNT network films can serve as hole collectors for PSCs without an organic HTM and Au electrode [201]; functionalized single-walled CNTs were embedded in an inert polymer matrix and achieved long-term stability in high-efficiency PSCs (Fig. 1.14g, h) [202]; transparent CNT electrodes were prepared for flexible PSCs based on a device structure of Ti foil/TiO_2 NTs/$MAPbI_3$/spiro-MeOTAD/CNTs [117]; CNT fiber electrodes were used to fabricate highly flexible, double-twisted PSCs with a maximum PCE of 3.03 % and performance stability longer than 96 h in open air as well as flexural stability for more than 1000 bending cycles [203].

1.2.6 Other Nanostructured Layers

Many other nanostructured materials, such as SnO_2 [61, 205–207], SiO_2 [66, 208, 209], Zn_2SnO_4 [210, 211], WO_x [63], $SrTiO_3$ [212], Nb_2O_5 [213], metal sulfides (i.e., PbS, $CuInS_2$, ZnS and CdS) [59, 214, 215], Cs_2CO_3 [216], $MoO_\times$ [217, 218], CuI [219], and CuSCN [220–222] have also been employed in the construction of PSC devices. Some representative examples are shown in the following section.

(1) SnO_2:Compared to TiO_2 and ZnO, SnO_2 has a similar band-gap, high transparency, and large electron mobility. However, SnO_2 has sufficient conductivity without a high temperature sintering process which is beneficial for the fabrication of flexible PSCs. Also, SnO_2 has a deeper conduction band (CB) than TiO_2 which facilitates a more efficient transfer of photo-generated electrons from the perovskite absorber to the SnO_2 CB. Furthermore, bulk SnO_2 has an electron mobility of up to 240 $cm^2\ V^{-1}\ s^{-1}$ which is 100 times higher than that of TiO_2 and promising for highly efficient solar cells [61, 205–207]. Thus, low-temperature solution-processed nanocrystalline SnO_2 films have been employed as the electron transporting layers (ETLs) in PSCs. Resulting devices achieved a peak PCE of 17.21 % (Fig. 1.15a–c) [61].

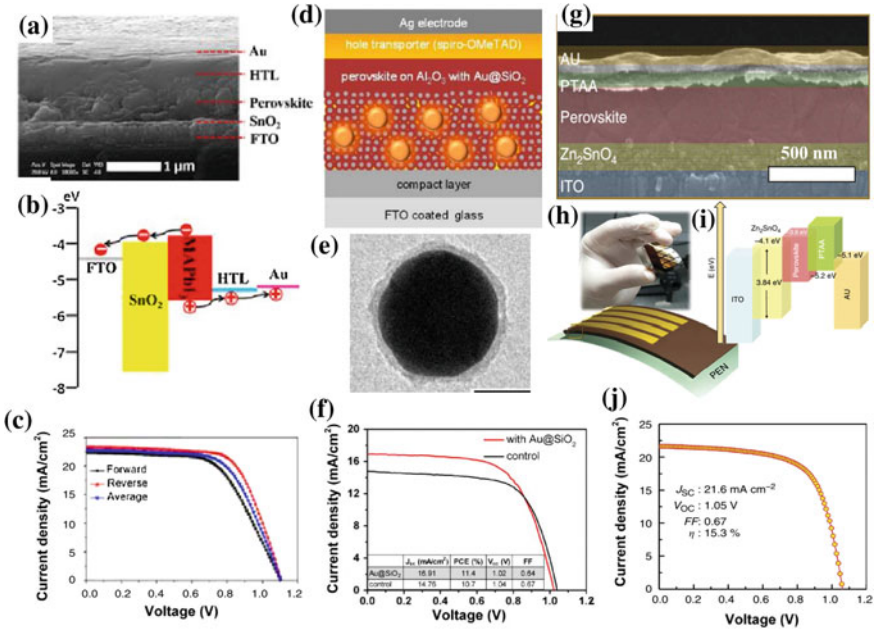

Fig. 1.15 Cross-sectional SEM images and energy band diagrams of the PSC devices based on **a**, **b** SnO_2 and **g**, **i** $ZnSnO_4$. I-V curves of the PSCs based on **c** SnO_2, **f** $Au@SiO_2$, and **j** $ZnSnO_4$. **e** TEM image of $Au@SiO_2$ NPs. **h** Photograph and of the $ZnSnO_4$-based flexible PSC (reprinted with permission from [61] **a**–**c** W. Ke et al., J. Am. Chem. Soc. 2015, 137, 6730–6733. [66] **d**–**f** W. Zhang et al., Nano Lett. 2013, 13, 4505–4510. [210] **g**–**j** S.S. Shin et al., Nature communications 2015, 6, 7410. Copyright © American Chemical Society and Nature Publishing Group)

(2) SiO_2: Similar to the insulating mesoporous Al_2O_3 scaffold, SiO_2 NPs were also employed as scaffold materials in PSCs. Resulting devices showed a PCE of up to 12.4 % [208, 209]. In particular, core-shell $Au@SiO_2$ NPs were incorporated into the Al_2O_3-based PSCs (Fig. 1.15d, e) and delivered a PCE of up to 11.4 % with enhanced J_{SC} (Fig. 1.15f). This is attributed to a reduced exciton binding energy and hence enhanced generation of free charge carriers with the incorporation of the metal NPs [66].

(3) Zn_2SnO_4: ZSO is an *n*-type semiconductor with a small electron effective mass of 0.23 m_e, a high electron Hall mobility of 10–30 $cm^2\ Vs^{-1}$, a wide optical band gap of 3.8 eV and a relatively low refractive index of $\sim$2.0 in the visible spectrum. Its conduction band edge is similar to TiO_2 and ZnO, making it an excellent electrode material in solar cell applications. More importantly, it has chemical stability with respect to acid/base solutions and polar organic solvents [210, 211]. Recently, dispersed ZSO NPs prepared at low-temperatures (<100 °C) were introduced into the development of flexible PSCs with a peak PCE of 15.3 % (Fig. 1.15g–j). This makes ZSO a promising candidate as an electron-conducting material for high efficiency flexible PSC applications [210].

1.3 Summary and Outlook

In this chapter, an overview of the historical progress in PSCs is presented. Next a focused review of the nanostructured materials used in the fabrication of PSCs is detailed. A summary of the development and prospects for several popular nanostructured materials; such as TiO_2, Al_2O_3 and ZnO, as well as other promising nanostructured materials, including NiO, carbon materials, metal sulfides, SnO_2, Zn_2SnO_4 is also outlined. These nanostructured materials can not only serve as effective blocking layers and scaffolds but can also play key roles in the HTM and novel metal electrodes in PSCs. In addition, these nanostructured inorganic materials can be used to modify the surface of perovskites and HTMs as well as the interface between them in order to improve the device efficiency and stability.

The high-efficiency, low material cost and simple assembly processes of PSCs make them economically viable for commercialization. More importantly, PSCs show promise for use in all-solid-state and flexible solar cells which are attractive power solutions for future wearable device technology. However, PSCs currently still face some challenges that hinder large-scale commercialization: (1) the toxicity of Pb atoms, (2) long-term stability, and (3) cost-effectiveness. In this regard, future research will aim at finding Pb-free perovskite materials, exploiting effective surface modification methods and external encapsulation technologies, and developing low cost materials and processes. It is probable that continued investigation of the nanostructured materials in PSCs will improve device stability and reduce the manufacturing costs of PSCs. If one thing is clear about PSCs, it is that the research and development of them in the last 6 years has been some of the most aggressive and effective of any technology. With ongoing challenges to push the PCE even higher, the trend in research will likely shift to one less focused on pushing the upper efficiency limit and more on the industrialization, scaling, fine tuning and repeatability of an already well-understood technology.

Acknowledgements This work was supported by the National Science Foundation (NSF ECCS-1305087), the National Nature Science Foundation of China (No.21503177), the Fundamental Research Funds for the Central Universities of China (No. 20720150031), and the 111 Project of China (B16029).

References

1. E. Serrano, G. Rus, J. García-Martínez, Nanotechnology for sustainable energy. Renew. Sustain. Energy Rev. **13**, 2373–2384 (2009)
2. N.S. Lewis, Toward cost-effective solar energy use. Science **315**, 798–801 (2007)
3. L. El Chaar, N. El Zein, Review of photovoltaic technologies. Renew. Sustain. Energy Rev. **15**, 2165–2175 (2011)
4. M. Grätzel, Recent advances in sensitized mesoscopic solar cells. Acc. Chem. Res. **42**, 1788–1798 (2009)
5. M.A. Green, Third generation photovoltaics: ultra-high conversion efficiency at low cost. Prog. Photovoltaics Res. Appl. **9**, 123–135 (2001)

6. Y.L. Lee, Y.S. Lo, Highly efficient quantum-dot-sensitized solar cell based on Co-sensitization of CdS/CdSe. Adv. Funct. Mater. **19**, 604–609 (2009)
7. S. Zhang, X. Yang, Y. Numata, L. Han, Highly efficient dye-sensitized solar cells: progress and future challenges. Energy Environ. Sci. **6**, 1443–1464 (2013)
8. N.-G. Park, Perovskite solar cells: an emerging photovoltaic technology. Mater. Today **18**, 65–72 (2014)
9. M. Gratzel, The light and shade of perovskite solar cells. Nat. Mater. **13**, 838–842 (2014)
10. M.D. McGehee, Perovskite solar cells: continuing to soar. Nat. Mater. **13**, 845–846 (2014)
11. G. Hodes, D. Cahen, Photovoltaics: Perovskite cells roll forward. Nat. Photon. **8**, 87–88 (2014)
12. M.A. Green, T. Bein, Photovoltaics Perovskite cells charge forward. Nat. Mater. **14**, 559–561 (2015)
13. N.-G. Park, Perovskite solar cells switchable photovoltaics. Nat. Mater. **14**, 140–141 (2015)
14. M.A. Green, A. Ho-Baillie, H.J. Snaith, The emergence of perovskite solar cells. Nat. Photonics **8**, 506–514 (2014)
15. G. Hodes, Perovskite-based solar cells. Science **342**, 317–318 (2013)
16. T.C. Sum, N. Mathews, Advancements in perovskite solar cells: photophysics behind the photovoltaics. Energy Environ. Sci. **7**, 2518–2534 (2014)
17. B.V. Lotsch, New light on an old story: Perovskites go solar. Angew. Chem. Int. Ed. **53**, 635–637 (2014)
18. M. Liu, M.B. Johnston, H.J. Snaith, Efficient planar heterojunction perovskite solar cells by vapour deposition. Nature **501**, 395–398 (2013)
19. M. Hu, L. Liu, A. Mei, Y. Yang, T. Liu, H. Han, Efficient hole-conductor-free, fully printable mesoscopic perovskite solar cells with a broad light harvester $NH_2CH{=}NH_2PbI_3$. J. Mater. Chem. A **2**, 17115–17121 (2014)
20. C.C. Stoumpos, C.D. Malliakas, M.G. Kanatzidis, Semiconducting tin and lead iodide perovskites with organic cations: phase transitions, high mobilities, and near-infrared photoluminescent properties. Inorg. Chem. **52**, 9019–9038 (2013)
21. J.H. Noh, S.H. Im, J.H. Heo, T.N. Mandal, S.I. Seok, Chemical management for colorful, efficient, and stable inorganic-organic hybrid nanostructured solar cells. Nano Lett. **13**, 1764–1769 (2013)
22. Y. Zhao, A.M. Nardes, K. Zhu, Mesoporous perovskite solar cells: material composition, charge-carrier dynamics, and device characteristics. Faraday Discuss. **176**, 301–312 (2014)
23. M. Jiang, J. Wu, F. Lan, Q. Tao, D. Gao, G. Li, Enhancing the performance of planar organo-lead halide perovskite solar cells by using a mixed halide source. J. Mater. Chem. A **3**, 963–967 (2015)
24. A. Kojima, K. Teshima, Y. Shirai, T. Miyasaka, Organometal halide perovskites as visible-light sensitizers for photovoltaic cells. J. Am. Chem. Soc. **131**, 6050–6051 (2009)
25. J.-H. Im, C.-R. Lee, J.-W. Lee, S.-W. Park, N.-G. Park, 6.5 % Efficient perovskite quantum-dot-sensitized solar cell. Nanoscale, **3**, 4088–4093 (2011)
26. H.-S. Kim, C.-R. Lee, J.-H. Im, K.-B. Lee, T. Moehl, A. Marchioro, S.-J. Moon, R. Humphry-Baker, J.-H. Yum, J.E. Moser, M. Graetzel, N.-G. Park. Lead iodide perovskite sensitized all-solid-state submicron thin film mesoscopic solar cell with efficiency exceeding 9 %. Sci. Rep., **2** (2012)
27. M.M. Lee, J. Teuscher, T. Miyasaka, T.N. Murakami, H.J. Snaith, Efficient hybrid solar cells based on meso-superstructured organometal halide perovskites. Science **338**, 643–647 (2012)
28. J.H. Heo, S.H. Im, J.H. Noh, T.N. Mandal, C.-S. Lim, J.A. Chang, Y.H. Lee, H.-J. Kim, A. Sarkar, M.K. Nazeeruddin, M. Graetzel, S.I. Seok, Efficient inorganic-organic hybrid heterojunction solar cells containing perovskite compound and polymeric hole conductors. Nat. Photonics **7**, 487–492 (2013)
29. J.M. Ball, M.M. Lee, A. Hey, H.J. Snaith, Low-temperature processed meso-superstructured to thin-film perovskite solar cells. Energy Environ. Sci. **6**, 1739–1743 (2013)

30. J. Burschka, N. Pellet, S.-J. Moon, R. Humphry-Baker, P. Gao, M.K. Nazeeruddin, M. Graetzel, Sequential deposition as a route to high-performance perovskite-sensitized solar cells. Nature **499**, 316–320 (2013)
31. S. Ryu, J.H. Noh, N.J. Jeon, Y. Chan Kim, W.S. Yang, J. Seo, S.I. Seok, Voltage output of efficient perovskite solar cells with high open-circuit voltage and fill factor. Energy Environ. Sci. **7**, 2614–2618 (2014)
32. N.J. Jeon, H.G. Lee, Y.C. Kim, J. Seo, J.H. Noh, J. Lee, S.I. Seok, o-Methoxy substituents in spiro-OMeTAD for efficient inorganic–organic hybrid perovskite solar cells. J. Am. Chem. Soc. **136**, 7837–7840 (2014)
33. T. Moehl, J.H. Im, Y.H. Lee, K. Domanski, F. Giordano, S.M. Zakeeruddin, M.I. Dar, L.-P. Heiniger, M.K. Nazeeruddin, N.-G. Park, M. Graetzel, Strong photocurrent amplification in perovskite solar cells with a porous TiO_2 blocking layer under reverse bias. J. Phys. Chem. Lett. **5**, 3931–3936 (2014)
34. H. Zhou, Q. Chen, G. Li, S. Luo, T.-B. Song, H.-S. Duan, Z. Hong, J. You, Y. Liu, Y. Yang, Interface engineering of highly efficient perovskite solar cells. Science **345**, 542–546 (2014)
35. W.S. Yang, J.H. Noh, N.J. Jeon, Y.C. Kim, S. Ryu, J. Seo, S.I. Seok, High-performance photovoltaic perovskite layers fabricated through intramolecular exchange. Science **348**, 1234–1237 (2015)
36. K.W. Tan, D.T. Moore, M. Saliba, H. Sai, L.A. Estroff, T. Hanrath, H.J. Snaith, U. Wiesner, Thermally induced structural evolution and performance of mesoporous block copolymer-directed alumina perovskite solar cells. ACS Nano **8**, 4730–4739 (2014)
37. Y. Deng, E. Peng, Y. Shao, Z. Xiao, Q. Dong, J. Huang, Scalable fabrication of efficient organolead trihalide perovskite solar cells with doctor-bladed active layers. Energy Environ. Sci. **8**, 1544–1550 (2015)
38. C. Law, L. Miseikis, S. Dimitrov, P. Shakya-Tuladhar, X. Li, P.R.F. Barnes, J. Durrant, B.C. O'Regan, Performance and stability of lead perovskite/TiO_2, polymer/PCBM, and dye sensitized solar cells at light intensities up to 70 Suns. Adv. Mater. **26**, 6268–6273 (2014)
39. B.-w. Park, B. Philippe, T. Gustafsson, K. Sveinbjornsson, A. Hagfeldt, E.M.J. Johansson, G. Boschloo, Enhanced crystallinity in organic-inorganic lead halide perovskites on mesoporous TiO_2 via disorder-order phase transition. Chem. Mater., **26**, 4466–4471 (2014)
40. J.-H. Im, J. Luo, M. Franckevicius, N. Pellet, P. Gao, T. Moehl, S.M. Zakeeruddin, M.K. Nazeeruddin, M. Graetzel, N.-G. Park, Nanowire perovskite solar cell. Nano Lett. **15**, 2120–2126 (2015)
41. N. Yantara, D. Sabba, F. Yanan, J.M. Kadro, T. Moehl, P.P. Boix, S. Mhaisalkar, M. Graetzel, C. Graetzel, Loading of mesoporous titania films by $CH_3NH_3PbI_3$ perovskite, single step vs. sequential deposition. Chem. Commun. **51**, 4603–4606 (2015)
42. W.C. Choy, Vacuum-assisted thermal annealing of $CH_3NH_3PbI_3$ for highly stable and efficient perovskite solar cells. ACS Nano **9**, 639–646 (2015)
43. D. Bi, A.M. El-Zohry, A. Hagfeldt, G. Boschloo, Unraveling the effect of PbI_2 concentration on charge recombination kinetics in perovskite solar cells. ACS Photonics **2**, 589–594 (2015)
44. T. Zhang, M. Yang, Y. Zhao, K. Zhu, Controllable sequential deposition of planar $CH_3NH_3PbI_3$ perovskite films via adjustable volume expansion. Nano Lett. **15**, 3959–3963 (2015)
45. T. Leijtens, G.E. Eperon, S. Pathak, A. Abate, M.M. Lee, H.J. Snaith, Overcoming ultraviolet light instability of sensitized TiO_2 with meso-superstructured organometal tri-halide perovskite solar cells. Nat. Commum. **4**, 2885 (2013)
46. A.K. Jena, H.-W. Chen, A. Kogo, Y. Sanehira, M. Ikegami, T. Miyasaka, The interface between FTO and the TiO_2 compact layer can be one of the origins to hysteresis in planar heterojunction perovskite solar cells. ACS Appl. Mater. Interfaces **7**, 9817–9823 (2015)
47. B. Suarez, V. Gonzalez-Pedro, T.S. Ripolles, R.S. Sanchez, L. Otero, I. Mora-Sero, Recombination study of combined halides (Cl, Br, I) perovskite solar cells. J. Phys. Chem. Lett. **5**, 1628–1635 (2014)

48. D. Bi, S.-J. Moon, L. Haggman, G. Boschloo, L. Yang, E.M.J. Johansson, M.K. Nazeeruddin, M. Graetzel, A. Hagfeldt, Using a two-step deposition technique to prepare perovskite ($CH_3NH_3PbI_3$) for thin film solar cells based on ZrO_2 and TiO_2 mesostructures. RSC Adv. **3**, 18762–18766 (2013)
49. J. Xiao, J. Shi, H. Liu, Y. Xu, S. Lv, Y. Luo, D. Li, Q. Meng, Y. Li, Efficient $CH_3NH_3PbI_3$ perovskite solar cells based on graphdiyne (GD)-modified P3HT hole-transporting material. Adv. Energy Mater. **5**, 1401943 (2015)
50. A. Abrusci, S.D. Stranks, P. Docampo, H.-L. Yip, A.K.Y. Jen, H.J. Snaith, High-performance perovskite-polymer hybrid solar cells via electronic coupling with fullerene monolayers. Nano Lett. **13**, 3124–3128 (2013)
51. J.-Y. Jeng, Y.-F. Chiang, M.-H. Lee, S.-R. Peng, T.-F. Guo, P. Chen, T.-C. Wen, $CH_3NH_3PbI_3$ Perovskite/fullerene planar-heterojunction hybrid solar cells. Adv. Mater. **25**, 3727–3732 (2013)
52. C. Kuang, G. Tang, T. Jiu, H. Yang, H. Liu, B. Li, W. Luo, X. Li, W. Zhang, F. Lu, J. Fang, Y. Li, Highly efficient electron transport obtained by doping PCBM with graphdiyne in planar-heterojunction perovskite solar cells. Nano Lett. **15**, 2756–2762 (2015)
53. N. Marinova, W. Tress, R. Humphry-Baker, M.I. Dar, V. Bojinov, S.M. Zakeeruddin, M.K. Nazeeruddin, M. Grätzel, Light harvesting and charge recombination in $CH_3NH_3PbI_3$ perovskite solar cells studied by hole transport layer thickness variation. ACS Nano **9**, 4200–4209 (2015)
54. H. Azimi, T. Ameri, H. Zhang, Y. Hou, C.O.R. Quiroz, J. Min, M. Hu, Z.G. Zhang, T. Przybilla, G.J. Matt, A universal interface layer based on an amine-functionalized fullerene derivative with dual functionality for efficient solution processed organic and perovskite solar cells. Adv. Energy Mater. **5**, 1401692 (2015)
55. S. Gamliel, L. Etgar, Organo-metal perovskite based solar cells: sensitized versus planar architecture. RSC Adv. **4**, 29012–29021 (2014)
56. H.-S. Kim, S.H. Im, N.-G. Park, Organolead halide perovskite: new horizons in solar cell research. J. Phys. Chem. C **118**, 5615–5625 (2014)
57. S. Luo, W.A. Daound, Recent progress in organic–inorganic halide perovskite solar cells: mechanisms and material design. J. Mater. Chem. A **3**, 8992–9010 (2015)
58. C.-W. Chen, H.-W. Kang, S.-Y. Hsiao, P.-F. Yang, K.-M. Chiang, H.-W. Lin, Efficient and uniform planar-type perovskite solar cells by simple sequential vacuum deposition. Adv. Mater. **26**, 6647–6652 (2014)
59. J. Liu, C. Gao, L. Luo, Q. Ye, X. He, L. Ouyang, X. Guo, D. Zhuang, C. Liao, J. Mei, W. Lau, Low-temperature, solution processed metal sulfide as an electron transport layer for efficient planar perovskite solar cells. J. Mater. Chem. A **3**, 11750–11755 (2015)
60. J.H. Park, J. Seo, S. Park, S.S. Shin, Y.C. Kim, N.J. Jeon, H.W. Shin, T.K. Ahn, J.H. Noh, S. C. Yoon, Efficient CH3NH3PbI3 perovskite solar cells employing nanostructured p-type NiO electrode formed by a pulsed laser deposition. Adv. Mater. **27**, 4013–4019 (2015)
61. W. Ke, G. Fang, Q. Liu, L. Xiong, P. Qin, H. Tao, J. Wang, H. Lei, B. Li, J. Wan, G. Yang, Y. Yan, Low-temperature solution-processed tin oxide as an alternative electron transporting layer for efficient perovskite solar cells. J. Am. Chem. Soc. **137**, 6730–6733 (2015)
62. A. Yella, L.-P. Heiniger, P. Gao, M.K. Nazeeruddin, M. Graetzel, Nanocrystalline rutile electron extraction layer enables low-temperature solution processed perovskite photovoltaics with 13.7 % efficiency. Nano Lett. **14**, 2591–2596 (2014)
63. K. Wang, Y. Shi, Q. Dong, Y. Li, S. Wang, X. Yu, M. Wu, T. Ma, Low-temperature and solution-processed amorphous WOX as electron-selective layer for perovskite solar cells. J. Phys. Chem. Lett. **6**, 755–759 (2015)
64. J. Zhang, P. Barboux, T. Pauporte, Electrochemical design of nanostructured ZnO charge carrier layers for efficient solid-state perovskite-sensitized solar cells. Adv. Energy Mater. **4**, 1400932 (2014)

65. H.-Y. Hsu, C.-Y. Wang, A. Fathi, J.-W. Shiu, C.-C. Chung, P.-S. Shen, T.-F. Guo, P. Chen, Y.-P. Lee, E.W.-G. Diau, Femtosecond excitonic relaxation dynamics of perovskite on mesoporous films of Al_2O_3 and NiO nanoparticles. Angew. Chem. Int. Ed. **53**, 9339–9342 (2014)
66. W. Zhang, M. Saliba, S.D. Stranks, Y. Sun, X. Shi, U. Wiesner, H.J. Snaith, Enhancement of perovskite-based solar cells employing core-shell metal nanoparticles. Nano Lett. **13**, 4505–4510 (2013)
67. L. Liu, A. Mei, T. Liu, P. Jiang, Y. Sheng, L. Zhang, H. Han, Fully printable mesoscopic perovskite solar cells with organic silane self-assembled monolayer. J. Am. Chem. Soc. **137**, 1790–1793 (2015)
68. X. Dong, X. Fang, M. Lv, B. Lin, S. Zhang, J. Ding, N. Yuan, Improvement of the humidity stability of organic-inorganic perovskite solar cells using ultrathin Al_2O_3 layers prepared by atomic layer deposition. J. Mater. Chem. A **3**, 5360–5367 (2015)
69. G. Murugadoss, G. Mizuta, S. Tanaka, H. Nishino, T. Umeyama, H. Imahori, S. Ito, Double functions of porous TiO_2 electrodes on $CH_3NH_3PbI_3$ perovskite solar cells: enhancement of perovskite crystal transformation and prohibition of short circuiting. APL Mater. **2**, 081511 (2014)
70. S.D. Sung, D.P. Ojha, J.S. You, J. Lee, J. Kim, W.I. Lee, 50 nm sized spherical TiO_2 nanocrystals for highly efficient mesoscopic perovskite solar cells. Nanoscale **7**, 8898–8906 (2015)
71. J. Song, J. Bian, E. Zheng, X.-F. Wang, W. Tian, T. Miyasaka, Efficient and environmentally stable perovskite solar cells based on ZnO electron collection layer. Chem. Lett. **44**, 610–612 (2015)
72. D.-Y. Son, K.-H. Bae, H.-S. Kim, N.-G. Park, Effects of seed layer on growth of ZnO nanorod and performance of perovskite solar cell. J. Phys. Chem. C **119**, 10321–10328 (2015)
73. S. Aharon, S. Gamliel, B.E. Cohen, L. Etgar, Depletion region effect of highly efficient hole conductor free $CH_3NH_3PbI_3$ perovskite solar cells. Phys. Chem. Chem. Phys. **16**, 10512–10518 (2014)
74. T. Leijtens, B. Lauber, G.E. Eperon, S.D. Stranks, H.J. Snaith, The importance of perovskite pore filling in organometal mixed halide sensitized TiO_2-based solar cells. J. Phys. Chem. Lett. **5**, 1096–1102 (2014)
75. J.-W. Lee, T.-Y. Lee, P.J. Yoo, M. Graetzel, S. Mhaisalkar, N.-G. Park, Rutile TiO_2-based perovskite solar cells. J. Mater. Chem. A **2**, 9251–9259 (2014)
76. S. Shi, Y. Li, X. Li, H. Wang, Advancements in all-solid-state hybrid solar cells based on organometal halide perovskites. Mater. Horiz. **2**, 378–405 (2015)
77. K. Wojciechowski, M. Saliba, T. Leijtens, A. Abate, H.J. Snaith, Sub-150 °C processed meso-superstructured perovskite solar cells with enhanced efficiency. Energy Environ. Sci. **7**, 1142–1147 (2014)
78. B. Conings, L. Baeten, T. Jacobs, R. Dera, J. D'Haen, J. Manca, H.-G. Boyen, An easy-to-fabricate low-temperature TiO_2 electron collection layer for high efficiency planar heterojunction perovskite solar cells. APL Mater. **2**, 081505 (2014)
79. W. Liu, Y. Zhang, Electrical characterization of $TiO_2/CH_3NH_3PbI_3$ heterojunction solar cells. J. Mater. Chem. A **2**, 10244–10249 (2014)
80. N.K. Noel, A. Abate, S.D. Stranks, E.S. Parrott, V.M. Burlakov, A. Goriely, H.J. Snaith, Enhanced photoluminescence and solar cell performance via Lewis base passivation of organic–inorganic lead halide perovskites. ACS Nano **8**, 9815–9821 (2014)
81. Y. Xiao, G. Han, Y. Li, M. Li, Y. Chang, J. Wu, Preparation of high performance perovskite-sensitized nanoporous titanium dioxide photoanodes by in situ method for use in perovskite solar cells. J. Mater. Chem. A **2**, 16531–16537 (2014)
82. Y. Xiao, G. Han, Y. Chang, Y. Zhang, Y. Li, M. Li, Investigation of perovskite-sensitized nanoporous titanium dioxide photoanodes with different thicknesses in perovskite solar cells. J. Power Sour. **286**, 118–123 (2015)

83. X. Wang, Y. Fang, L. He, Q. Wang, T. Wu, Influence of compact TiO_2 layer on the photovoltaic characteristics of the organometal halide perovskite-based solar cells. Mater. Sci. Semicond. Process. **27**, 569–576 (2014)
84. P. Qin, S. Tanaka, S. Ito, N. Tetreault, K. Manabe, H. Nishino, M.K. Nazeeruddin, M. Grätzel, Inorganic hole conductor-based lead halide perovskite solar cells with 12.4 % conversion efficiency. Nat. Commun., **5** (2014)
85. W. Li, H. Dong, X. Guo, N. Li, J. Li, G. Niu, L. Wang, Graphene oxide as dual functional interface modifier for improving wettability and retarding recombination in hybrid perovskite solar cells. J. Mater. Chem. A (2014)
86. F. Di Giacomo, V. Zardetto, A. D'Epifanio, S. Pescetelli, F. Matteocci, S. Razza, A. Di Carlo, S. Licoccia, W.M.M. Kessels, M. Creatore, T.M. Brown, Flexible perovskite photovoltaic modules and solar cells based on atomic layer deposited compact layers and UV-irradiated TiO_2 scaffolds on plastic substrates. Adv. Energy Mater. **5**, 1401808 (2015)
87. Y. Wu, X. Yang, H. Chen, K. Zhang, C. Qin, J. Liu, W. Peng, A. Islam, E. Bi, F. Ye, M. Yin, P. Zhang, L. Han, Highly compact TiO_2 layer for efficient hole-blocking in perovskite solar cells. Appl. Phys. Express **7**, 052301 (2014)
88. W. Ke, G. Fang, J. Wang, P. Qin, H. Tao, H. Lei, Q. Liu, X. Dai, X. Zhao, Perovskite solar cell with an efficient TiO_2 compact film. ACS Appl. Mater. Interfaces **6**, 15959–15965 (2014)
89. Q. Gao, S. Yang, L. Lei, S. Zhang, Q. Cao, J. Xie, J. Li, Y. Liu, An effective TiO_2 blocking layer for perovskite solar cells with enhanced performance. Chem. Lett. **44**, 624–626 (2015)
90. S.D. Sung, M.S. Kang, I.T. Choi, H.M. Kim, H. Kim, M. Hong, H.K. Kim, W.I. Lee, 14.8 % perovskite solar cells employing carbazole derivatives as hole transporting materials. Chem. Commun. **50**, 14161–14163 (2014)
91. S. Das, B. Yang, G. Gu, P.C. Joshi, I.N. Ivanov, C.M. Rouleau, T. Aytug, D.B. Geohegan, K. Xiao, High-performance flexible perovskite solar cells by using a combination of ultrasonic spray-coating and low thermal budget photonic curing. ACS Photonics **2**, 680–686 (2015)
92. S. Hong, A. Han, E.C. Lee, K.-W. Ko, J.-H. Park, H.-J. Song, M.-H. Han, C.-H. Han, A facile and low-cost fabrication of TiO_2 compact layer for efficient perovskite solar cells. Curr. Appl. Phys. **15**, 574–579 (2015)
93. S. Ameen, M.S. Akhtar, H.-K. Seo, M.K. Nazeeruddin, H.-S. Shin, Exclusion of metal oxide by an RF sputtered Ti layer in flexible perovskite solar cells: energetic interface between a Ti layer and an organic charge transporting layer. Dalton Trans. **44**, 6439–6448 (2015)
94. M. Lee, Y. Jo, D.S. Kim, Y. Jun, Flexible organo-metal halide perovskite solar cells on a Ti metal substrate. J. Mater. Chem. A **3**, 4129–4133 (2015)
95. L. Cojocaru, S. Uchida, Y. Sanehira, J. Nakazaki, T. Kubo, H. Segawa, Surface treatment of the compact TiO_2 layer for efficient planar heterojunction peroyskite solar cells. Chem. Lett. **44**, 674–676 (2015)
96. J. Wang, M. Qin, H. Tao, W. Ke, Z. Chen, J. Wan, P. Qin, L. Xiong, H. Lei, H. Yu, G. Fang, Performance enhancement of perovskite solar cells with Mg-doped TiO_2 compact film as the hole-blocking layer. Appl. Phys. Lett. **106**, 121104 (2015)
97. T. Krishnamoorthy, F. Kunwu, P.P. Boix, H. Li, T.M. Koh, W.L. Leong, S. Powar, A. Grimsdale, M. Gratzel, N. Mathews, S.G. Mhaisalkar, A swivel-cruciform thiophene based hole-transporting material for efficient perovskite solar cells. J. Mater. Chem. A **2**, 6305–6309 (2014)
98. K. Do, H. Choi, K. Lim, H. Jo, J.W. Cho, M.K. Nazeeruddin, J. Ko, Star-shaped hole transporting materials with a triazine unit for efficient perovskite solar cells. Chem. Commun. **50**, 10971–10974 (2014)
99. P. Qin, N. Tetreault, M.I. Dar, P. Gao, K.L. McCall, S.R. Rutter, S.D. Ogier, N.D. Forrest, J.S. Bissett, M.J. Simms, A.J. Page, R. Fisher, M. Grätzel, M.K. Nazeeruddin, A novel oligomer as a hole transporting material for efficient perovskite solar cells. Adv. Energy Mater. **5**, 1400980 (2014)

100. Z. Zhu, Y. Bai, H.K.H. Lee, C. Mu, T. Zhang, L. Zhang, J. Wang, H. Yan, S.K. So, S. Yang, Polyfluorene derivatives are high-performance organic hole-transporting materials for inorganic–organic hybrid perovskite solar cells. Adv. Funct. Mater. **24**, 7357–7365 (2014)
101. N. Fu, C. Huang, Y. Liu, X. Li, W. Lu, L. Zhou, F. Peng, Y. Liu, H. Huang, Organic-free anatase TiO_2 paste for efficient plastic dye-sensitized solar cells and low temperature processed perovskite solar cells. ACS Appl. Mater. Interfaces **7**, 19431–19438 (2015)
102. S.D. Stranks, G.E. Eperon, G. Grancini, C. Menelaou, M.J.P. Alcocer, T. Leijtens, L.M. Herz, A. Petrozza, H.J. Snaith, Electron-hole diffusion lengths exceeding 1 micrometer in an organometal trihalide perovskite absorber. Science **342**, 341–344 (2013)
103. S. Kazim, M.K. Nazeeruddin, M. Grätzel, S. Ahmad, Perovskite as light harvester: a game changer in photovoltaics. Angew. Chem. Int. Ed. **53**, 2812–2824 (2014)
104. Q. Jiang, X. Sheng, Y. Li, X. Feng, T. Xu, Rutile TiO_2 nanowire-based perovskite solar cells. Chem. Commun. **50**, 14720–14723 (2014)
105. F. Hao, C.C. Stoumpos, D.H. Cao, R.P.H. Chang, M.G. Kanatzidis, Lead-free solid-state organic-inorganic halide perovskite solar cells. Nat. Photon. **8**, 489–494 (2014)
106. P. Qin, S. Paek, M.I. Dar, N. Pellet, J. Ko, M. Grätzel, M.K. Nazeeruddin, Perovskite solar cells with 12.8 % efficiency by using conjugated quinolizino acridine based hole transporting material. J. Am. Chem. Soc. **136**, 8516–8519 (2014)
107. Z. Zhu, J. Ma, Z. Wang, C. Mu, Z. Fan, L. Du, Y. Bai, L. Fan, H. Yan, D.L. Phillips, S. Yang, Efficiency enhancement of perovskite solar cells through fast electron extraction: the role of graphene quantum dots. J. Am. Chem. Soc. **136**, 3760–3763 (2014)
108. Y. Yang, K. Ri, A. Mei, L. Liu, M. Hu, T. Liu, X. Li, H. Han, The size effect of TiO_2 nanoparticles on a printable mesoscopic perovskite solar cell. J. Mater. Chem. A **3**, 9103–9107 (2015)
109. C.B. Zhong D, Wang X, et al., Synthesis of oriented TiO_2 nanocones with fast charge transfer for perovskite solar cells. Nano Energy, **11**, 409–418 (2015)
110. X. Gao, J. Li, J. Baker, Y. Hou, D. Guan, J. Chen, C. Yuan, Enhanced photovoltaic performance of perovskite $CH_3NH_3PbI_3$ solar cells with freestanding TiO_2 nanotube array films. Chem. Commun. **50**, 6368–6371 (2014)
111. S. Dharani, H.K. Mulmudi, N. Yantara, T. Pham Thi Thu, N.G. Park, M. Graetzel, S. Mhaisalkar, N. Mathews, P.P. Boix, High efficiency electrospun TiO_2 nanofiber based hybrid organic-inorganic perovskite solar cell. Nanoscale **6**, 1675–1679 (2014)
112. H.-S. Kim, J.-W. Lee, N. Yantara, P.P. Boix, S.A. Kulkarni, S. Mhaisalkar, M. Graetzel, N.-G. Park, High efficiency solid-state sensitized solar cell-based on submicrometer rutile TiO_2 nanorod and $CH_3NH_3PbI_3$ perovskite sensitizer. Nano Lett. **13**, 2412–2417 (2013)
113. J. Qiu, Y. Qiu, K. Yan, M. Zhong, C. Mu, H. Yan, S. Yang, All-solid-state hybrid solar cells based on a new organometal halide perovskite sensitizer and one-dimensional TiO_2 nanowire arrays. Nanoscale **5**, 3245–3248 (2013)
114. D. Zhong, B. Cai, Z. Yang, B. Huang, S. Miao, W-H. Zhang, J. Qiu, C. Li, An acid-free medium growth of rutile TiO_2 nanorods arrays and their application in perovskite solar cells. J. Mater. Chem. C, **3**, 729–733 (2015)
115. A. Fakharuddin, F. Di Giacomo, I. Ahmed, Q. Wali, T.M. Brown, R. Jose, Role of morphology and crystallinity of nanorod and planar electron transport layers on the performance and long term durability of perovskite solar cells. J. Power Sour. **283**, 61–67 (2015)
116. S.S. Mali, C.S. Shim, H.K. Park, J. Heo, P.S. Patil, C.K. Hong, Ultrathin atomic layer deposited TiO_2 for surface passivation of hydrothermally grown 1D TiO_2 nanorod arrays for efficient solid-state perovskite solar cells. Chem. Mater. **27**, 1541–1551 (2015)
117. X. Wang, Z. Li, W. Xu, S.A. Kulkarni, S.K. Batabyal, S. Zhang, A. Cao, L.H. Wong, TiO_2 nanotube arrays based flexible perovskite solar cells with transparent carbon nanotube electrode. Nano Energy **11**, 728–735 (2015)
118. D. Zhong, B. Cai, X. Wang, Z. Yang, Y. Xing, S. Miao, W.-H. Zhang, C. Li, Synthesis of oriented TiO_2 nanocones with fast charge transfer for perovskite solar cells. Nano Energy **11**, 409–418 (2015)

119. R. Salazar, M. Altomare, K. Lee, J. Tripathy, R. Kirchgeorg, N.T. Nguyen, M. Mokhtar, A. Alshehri, S.A. Al-Thabaiti, P. Schmuki, Use of anodic TiO_2 nanotube layers as mesoporous scaffolds for fabricating $CH_3NH_3PbI_3$ perovskite-based solid-state solar cells. ChemElectroChem (2015)
120. J. Zhang, T. Pauporté, One-dimensional self-standing TiO_2 nanotube array layers designed for perovskite solar cell applications. ChemPhysChem **16**, 2836–2841 (2015)
121. H. Yang, W. Fang, X. Yang, H. Zhu, Z. Li, H. Zhao, X. Yao, Yolk@ shell anatase TiO_2 hierarchical microspheres with exposed 001 facets for high-performance dye sensitized solar cells. J. Mater. Chem. **22**, 22082–22089 (2012)
122. W. Yang, J. Li, Y. Wang, F. Zhu, W. Shi, F. Wan, D. Xu, A facile synthesis of anatase TiO_2 nanosheets-based hierarchical spheres with over 90 %{001} facets for dye-sensitized solar cells. Chem. Commun. **47**, 1809–1811 (2011)
123. J.G. Yu, J.J. Fan, K.L. Lv, Anatase TiO_2 nanosheets with exposed (001) facets: improved photoelectric conversion efficiency in dye-sensitized solar cells. Nanoscale **2**, 2144–2149 (2010)
124. Y. Rong, Z. Ku, A. Mei, T. Liu, M. Xu, S. Ko, X. Li, H. Han, Hole-conductor-free mesoscopic $TiO_2/CH_3NH_3PbI_3$ heterojunction solar cells based on anatase nanosheets and carbon counter electrodes. J. Phys. Chem. Lett. **5**, 2160–2164 (2014)
125. M.I. Dar, F.J. Ramos, Z. Xue, B. Liu, S. Ahmad, S.A. Shivashankar, M.K. Nazeeruddin, M. Graetzel, Photoanode based on (001)-oriented anatase nanoplatelets for organic-inorganic lead iodide perovskite solar cell. Chem. Mater. **26**, 4675–4678 (2014)
126. J.-W. Lee, S.H. Lee, H.-S. Ko, J. Kwon, J.H. Park, S.M. Kang, N. Ahn, M. Choi, J.K. Kim, N.-G. Park, Opto-electronic properties of TiO_2 nanohelices with embedded $HC(NH_2)_2PbI_3$ perovskite solar cells. J. Mater. Chem. A **3**, 9179–9186 (2015)
127. W.Q. Wu, F. Huang, D. Chen, Y.B. Cheng, R.A. Caruso, Thin films of dendritic anatase titania nanowires enable effective hole-blocking and efficient light-harvesting for high-performance mesoscopic perovskite solar cells. Adv. Funct. Mater. **25**, 3264–3272 (2015)
128. H. Sun, P. Ruan, Z. Bao, L. Chen, X. Zhou, Shell-in-shell TiO_2 hollow microspheres and optimized application in light-trapping perovskite solar cells. Solid State Sci. **40**, 60–66 (2015)
129. K. Mahmood, B.S. Swain, A. Amassian, Highly efficient hybrid photovoltaics based on hyperbranched three-dimensional TiO_2 electron transporting materials. Adv. Mater. **27**, 2859–2865 (2015)
130. Y. Yu, J. Li, D. Geng, J. Wang, L. Zhang, T.L. Andrew, M.S. Arnold, X. Wang, Development of lead iodide perovskite solar cells using three-dimensional titanium dioxide nanowire architectures. ACS Nano **9**, 564–572 (2015)
131. S.K. Pathak, A. Abate, P. Ruckdeschel, B. Roose, K.C. Goedel, Y. Vaynzof, A. Santhala, S.-I. Watanabe, D.J. Hollman, N. Noel, A. Sepe, U. Wiesner, R. Friend, H.J. Snaith, U. Steiner, Performance and stability enhancement of dye-sensitized and perovskite solar cells by Al doping of TiO_2. Adv. Funct. Mater. **24**, 6046–6055 (2014)
132. M. Yang, R. Guo, K. Kadel, Y. Liu, K. O'Shea, R. Bone, X. Wang, J. He, W. Li, Improved charge transport of Nb-doped TiO_2 nanorods in methylammonium lead iodide bromide perovskite solar cells. J. Mater. Chem. A **2**, 19616–19622 (2014)
133. Z. Yuan, Z. Wu, S. Bai, Z. Xia, W. Xu, T. Song, H. Wu, L. Xu, J. Si, Y. Jin, B. Sun, Hot-electron injection in a sandwiched TiOx-Au-TiOx structure for high-performance planar perovskite solar cells. Adv. Energy Mater. **5**, 1500038 (2015)
134. G.S. Han, H.S. Chung, B.J. Kim, D.H. Kim, J.W. Lee, B.S. Swain, K. Mahmood, J.S. Yoo, N.-G. Park, J.H. Lee, Retarding charge recombination in perovskite solar cells using ultrathin MgO-coated TiO_2 nanoparticulate films. J. Mater. Chem. A **3**, 9160–9164 (2015)
135. B.S. Swain, K. Mahmood, A.R. Kirmani et al., Highly efficient perovskite solar cells based on a nanostructured WO_3–TiO_2 core–shell electron transporting material. J. Mater. Chem. A, **3**, 9051–9057 (2015)

136. H.B. Kim, I. Im, Y. Yoon, S.D. Sung, E. Kim, J. Kim, W.I. Lee, Enhancement of photovoltaic properties of CH3NH3PbBr 3 heterojunction solar cells by modifying mesoporous TiO_2 surfaces with carboxyl groups. J. Mater. Chem. A **3**, 9264–9270 (2015)
137. J. Kwon, S.J. Kim, J.H. Park, The tailored inner space of TiO_2 electrodes via a 30 second wet etching process: high efficiency solid-state perovskite solar cells. Nanoscale **7**, 10745–10751 (2015)
138. P. Qin, A.L. Domanski, A.K. Chandiran, R. Berger, H.-J. Butt, M.I. Dar, T. Moehl, N. Tetreault, P. Gao, S. Ahmad, M.K. Nazeeruddin, M. Gratzel, Yttrium-substituted nanocrystalline TiO_2 photoanodes for perovskite based heterojunction solar cells. Nanoscale **6**, 1508–1514 (2014)
139. H.-H. Wang, Q. Chen, H. Zhou, L. Song, Z. St Louis, N. De Marco, Y. Fang, P. Sun, T.-B. Song, H. Chen, Y. Yang, Improving the TiO_2 electron transport layer in perovskite solar cells using acetylacetonate-based additives. J. Mater. Chem. A, **3**, 9108–9115 (2015)
140. H. Nagaoka, F. Ma, D.W. deQuilettes, S.M. Vorpahl, M.S. Glaz, A.E. Colbert, M.E. Ziffer, D.S. Ginger, Zr incorporation into TiO_2 electrodes reduces hysteresis and improves performance in hybrid perovskite solar cells while increasing carrier lifetimes. J. Phys. Chem. Lett. **6**, 669–675 (2015)
141. X. Zhang, Z. Bao, X. Tao, H. Sun, W. Chen, X. Zhou, Sn-doped TiO_2 nanorod arrays and application in perovskite solar cells. RSC Adv. **4**, 64001–64005 (2014)
142. K. Manseki, T. Ikeya, A. Tamura, T. Ban, T. Sugiura, T. Yoshida, Mg-doped TiO_2 nanorods improving open-circuit voltages of ammonium lead halide perovskite solar cells. RSC Adv. **4**, 9652–9655 (2014)
143. J.T.-W. Wang, J.M. Ball, E.M. Barea, A. Abate, J.A. Alexander-Webber, J. Huang, M. Saliba, I. Mora-Sero, J. Bisquert, H.J. Snaith, R.J. Nicholas, Low-temperature processed electron collection layers of graphene/TiO_2 nanocomposites in thin film perovskite solar cells. Nano Lett. **14**, 724–730 (2014)
144. S. Ito, S. Tanaka, K. Manabe, H. Nishino, Effects of surface blocking layer of Sb_2S_3 on nanocrystalline TiO_2 for $CH_3NH_3PbI_3$ perovskite solar cells. J. Phys. Chem. C **118**, 16995–17000 (2014)
145. X. Xu, Z. Liu, Z. Zuo, M. Zhang, Z. Zhao, Y. Shen, H. Zhou, Q. Chen, Y. Yang, M. Wang, Hole selective NiO contact for efficient perovskite solar cells with carbon electrode. Nano Lett. **15**, 2402–2408 (2015)
146. L. Zhang, T. Liu, L. Liu, M. Hu, Y. Yang, A. Mei, H. Han, The effect of carbon counter electrodes on fully printable mesoscopic perovskite solar cells. J. Mater. Chem. A **3**, 9165–9170 (2015)
147. X. Guo, H. Dong, W. Li, N. Li, L. Wang, Multifunctional MgO layer in perovskite solar cells. ChemPhysChem **16**, 1727–1732 (2015)
148. M.J. Carnie, C. Charbonneau, M.L. Davies, J. Troughton, T.M. Watson, K. Wojciechowski, H. Snaith, D.A. Worsley, A one-step low temperature processing route for organolead halide perovskite solar cells. Chem. Commun. **49**, 7893–7895 (2013)
149. W. Li, J. Li, L. Wang, G. Niu, R. Gao, Y. Qiu, Post modification of perovskite sensitized solar cells by aluminum oxide for enhanced performance. J. Mater. Chem. A **1**, 11735–11740 (2013)
150. G. Niu, W. Li, F. Meng, L. Wang, H. Dong, Y. Qiu, Study on the stability of $CH_3NH_3PbI_3$ films and the effect of post-modification by aluminum oxide in all-solid-state hybrid solar cells. J. Mater. Chem. A **2**, 705–710 (2014)
151. S. Guarnera, A. Abate, W. Zhang, J.M. Foster, G. Richardson, A. Petrozza, H.J. Snaith, Improving the long-term stability of perovskite solar cells with a porous Al_2O_3 buffer-layer. J. Phys. Chem. Lett. (2015)
152. S. Guarnera, A. Abate, W. Zhang, J.M. Foster, G. Richardson, A. Petrozza, H.J. Snaith, Improving the long-term stability of perovskite solar cells with a porous Al_2O_3 buffer layer. J. Phys. Chem. Lett. **6**, 432–437 (2015)

153. S.N. Habisreutinger, T. Leijtens, G.E. Eperon, S.D. Stranks, R.J. Nicholas, H.J. Snaith, Carbon nanotube/polymer composites as a highly stable hole collection layer in perovskite solar cells. Nano Lett. **14**, 5561–5568 (2014)
154. H. Wei, J. Shi, X. Xu, J. Xiao, J. Luo, J. Dong, S. Lv, L. Zhu, H. Wu, D. Li, Y. Luo, Q. Meng, Q. Chen, Enhanced charge collection with ultrathin AlO_x electron blocking layer for hole-transporting material-free perovskite solar cell. Phys. Chem. Chem. Phys. **17**, 4937–4944 (2015)
155. A. Listorti, E.J. Juarez-Perez, C. Frontera, V. Roiati, L. Garcia-Andrade, S. Colella, A. Rizzo, P. Ortiz, I. Mora-Sero, Effect of mesostructured layer upon crystalline properties and device performance on perovskite solar cells. J. Phys. Chem. Lett. **6**, 1628–1637 (2015)
156. J.-J. Shi, W. Dong, Y.-Z. Xu, C.-H. Li, S.-T. Lv, L.-F. Zhu, J. Dong, Y.-H. Luo, D.-M. Li, Q.-B. Meng, Q. Chen, Enhanced performance in perovskite organic lead iodide heterojunction solar cells with metal-insulator-semiconductor back contact. Chin. Phys. Lett. **30**, 128402 (2013)
157. M.M. Tavakoli, K.-H. Tsui, Q. Zhang, J. He, Y. Yao, D. Li, Z. Fan, Highly efficient flexible perovskite solar cells with antireflection and self-cleaning nanostructures. ACS Nano **9**, 10287–10295 (2015)
158. D. Liu, T.L. Kelly, Perovskite solar cells with a planar heterojunction structure prepared using room-temperature solution processing techniques. Nat. Photonics **8**, 133–138 (2014)
159. J. Kim, G. Kim, T.K. Kim, S. Kwon, H. Back, J. Lee, S.H. Lee, H. Kang, K. Lee, Efficient planar-heterojunction perovskite solar cells achieved via interfacial modification of a sol-gel ZnO electron collection layer. J. Mater. Chem. A **2**, 17291–17296 (2014)
160. H. Zhou, Y. Shi, K. Wang, Q. Dong, X. Bai, Y. Xing, Y. Du, T. Ma, Low-temperature processed and carbon-based ZnO/CH(3)NH(3)Pbl(3)/C planar heterojunction perovskite solar cells. J. Phys. Chem. C **119**, 4600–4605 (2015)
161. D. Bi, G. Boschloo, S. Schwarzmueller, L. Yang, E.M.J. Johansson, A. Hagfeldt, Efficient and stable $CH_3NH_3PbI_3$-sensitized ZnO nanorod array solid-state solar cells. Nanoscale **5**, 11686–11691 (2013)
162. D.-Y. Son, J.-H. Im, H.-S. Kim, N.-G. Park, 11% efficient perovskite solar cell based on ZnO nanorods: an effective charge collection system. J. Phys. Chem. C **118**, 16567–16573 (2014)
163. X. Dong, H. Hu, B. Lin, J. Ding, N. Yuan, The effect of ALD-Zno layers on the formation of $CH_3NH_3PbI_3$ with different perovskite precursors and sintering temperatures. Chem. Commun. **50**, 14405–14408 (2014)
164. D. Liu, J. Yang, T.L. Kelly, Compact layer free perovskite solar cells with 13.5 % efficiency. J. Am. Chem. Soc. **136**, 17116–17122 (2014)
165. Y. Cheng, Q.-D. Yang, J. Xiao, Q. Xue, H.-W. Li, Z. Guan, H.-L. Yip, S.-W. Tsang, Decomposition of organometal halide perovskite films on zinc oxide nanoparticles. ACS Appl. Mater. Interfaces **7**, 19986–19993 (2015)
166. K. Mahmood, B.S. Swain, A. Amassian, Double-layered ZnO nanostructures for efficient perovskite solar cells. Nanoscale **6**, 14674–14678 (2014)
167. S. Ameen, M.S. Akhtar, H.-K. Seo, M.K. Nazeeruddin, H.-S. Shin, An insight into atmospheric plasma jet modified ZnO quantum dots thin film for flexible perovskite solar cell: optoelectronic transient and charge trapping studies. J. Phys. Chem. C **119**, 10379–10390 (2015)
168. K. Mahmood, B.S. Swain, H.S. Jung, Controlling the surface nanostructure of ZnO and Al-doped ZnO thin films using electrostatic spraying for their application in 12 % efficient perovskite solar cells. Nanoscale **6**, 9127–9138 (2014)
169. J. Han, S. Yuan, L. Liu, X. Qiu, H. Gong, X. Yang, C. Li, Y. Hao, B. Cao, Fully indium-free flexible Ag nanowires/ZnO: F composite transparent conductive electrodes with high haze. J. Mater. Chem. A **3**, 5375–5384 (2015)
170. J. Dong, Y. Zhao, J. Shi, H. Wei, J. Xiao, X. Xu, J. Luo, J. Xu, D. Li, Y. Luo, Q. Meng, Impressive enhancement in the cell performance of ZnO nanorod-based perovskite solar cells with Al-doped ZnO interfacial modification. Chem. Commun. **50**, 13381–13384 (2014)

171. K. Mahmood, B. S. Swain, A. Amassian, 16.1 % efficient hysteresis-free mesostructured perovskite solar cells based on synergistically improved ZnO nanorod arrays. Adv. Energy Mater., **5**, 1500568 (2015)
172. K. Hwang, Y.S. Jung, Y.J. Heo, F.H. Scholes, S.E. Watkins, J. Subbiah, D.J. Jones, D.Y. Kim, D. Vak, Toward large scale roll-to-roll production of fully printed perovskite solar cells. Adv. Mater. **27**, 1241–1247 (2015)
173. S. He, L. Qiu, X. Fang, G. Guan, P. Chen, Z. Zhang, H. Peng, Radically grown obelisk-like ZnO arrays for perovskite solar cell fibers and fabrics through a mild solution process. J. Mater. Chem. A **3**, 9406–9410 (2015)
174. J.-Y. Jeng, K.-C. Chen, T.-Y. Chiang, P.-Y. Lin, T.-D. Tsai, Y.-C. Chang, T.-F. Guo, P. Chen, T.-C. Wen, Y.-J. Hsu, Nickel oxide electrode interlayer in $CH_3NH_3PbI_3$ perovskite/PCBM planar-heterojunction hybrid solar cells. Adv. Mater. **26**, 4107–4113 (2014)
175. K.-C. Wang, J.-Y. Jeng, P.-S. Shen, Y.-C. Chang, E.W.-G. Diau, C.-H. Tsai, T.-Y. Chao, H.-C. Hsu, P.-Y. Lin, P. Chen, T.-F. Guo, T.-C. Wen. *p*-Type mesoscopic nickel oxide/organometallic perovskite heterojunction solar cells. Sci. Rep., **4** (2014)
176. L. Hu, J. Peng, W. Wang, Z. Xia, J. Yuan, J. Lu, X. Huang, W. Ma, H. Song, W. Chen, Y.-B. Cheng, J. Tang, Sequential deposition of $CH_3NH_3PbI_3$ on planar NiO film for efficient planar perovskite solar cells. ACS Photonics **1**, 547–553 (2014)
177. Z. Zhu, Y. Bai, T. Zhang, Z. Liu, X. Long, Z. Wei, Z. Wang, L. Zhang, J. Wang, F. Yan, S. Yang, High-performance hole-extraction layer of sol-gel-processed NiO nanocrystals for inverted planar perovskite solar cells. Angew. Chem. Int. Ed. **53**, 12571–12575 (2014)
178. J. Cui, F. Meng, H. Zhang, K. Cao, H. Yuan, Y. Cheng, F. Huang, M. Wang, $CH_3NH_3PbI_3$-based planar solar cells with magnetron-sputtered nickel oxide. ACS Appl. Mater. Interfaces **6**, 22862–22870 (2014)
179. K.-C. Wang, P.-S. Shen, M.-H. Li, S. Chen, M.-W. Lin, P. Chen, T.-F. Guo, Low-temperature sputtered nickel oxide compact thin film as effective electron blocking layer for mesoscopic $NiO/CH_3NH_3PbI_3$ perovskite heterojunction solar cells. ACS Appl. Mater. Interfaces **6**, 11851–11858 (2014)
180. H. Tian, B. Xu, H. Chen, E.M.J. Johansson, G. Boschloo, Solid-state perovskite-sensitized *p*-type mesoporous nickel oxide solar cells. ChemSusChem **7**, 2150–2153 (2014)
181. H. Wang, X. Zeng, Z. Huang, W. Zhang, X. Qiao, B. Hu, X. Zou, M. Wang, Y.-B. Cheng, W. Chen, Boosting the photocurrent density of *p*-type solar cells based on organometal halide perovskite-sensitized mesoporous NiO photocathodes. ACS Appl. Mater. Interfaces **6**, 12609–12617 (2014)
182. J.H. Kim, P.-W. Liang, S.T. Williams, N. Cho, C.-C. Chueh, M.S. Glaz, D.S. Ginger, A.K.Y. Jen, High-performance and environmentally stable planar heterojunction perovskite solar cells based on a solution-processed copper-doped nickel oxide hole-transporting layer. Adv. Mater. **27**, 695–701 (2015)
183. Z. Liu, M. Zhang, X. Xu, L. Bu, W. Zhang, W. Li, Z. Zhao, M. Wang, Y.-B. Cheng, H. He, *p*-Type mesoscopic NiO as an active interfacial layer for carbon counter electrode based perovskite solar cells. Dalton Trans. **44**, 3967–3973 (2015)
184. W. Chen, Y. Wu, J. Liu, C. Qin, X. Yang, A. Islam, Y.-B. Cheng, L. Han, Hybrid interfacial layer leads to solid performance improvement of inverted perovskite solar cells. Energy Environ. Sci. **8**, 629–640 (2015)
185. Y. Bai, H. Yu, Z. Zhu, K. Jiang, T. Zhang, N. Zhao, S. Yang, H. Yan, High performance inverted structure perovskite solar cells based on a PCBM: polystyrene blend electron transport layer. J. Mater. Chem. A **3**, 9098–9102 (2015)
186. M.F. De Volder, S.H. Tawfick, R.H. Baughman, A.J. Hart, Carbon nanotubes: present and future commercial applications. Science **339**, 535–539 (2013)
187. D.S. Hecht, L. Hu, G. Irvin, Emerging transparent electrodes based on thin films of carbon nanotubes, graphene, and metallic nanostructures. Adv. Mater. **23**, 1482–1513 (2011)

188. W. Li, H. Dong, X. Guo, N. Li, J. Li, G. Niu, L. Wang, Graphene oxide as dual functional interface modifier for improving wettability and retarding recombination in hybrid perovskite solar cells. J. Mater. Chem. A **2**, 20105–20111 (2014)
189. Z. Wu, S. Bai, J. Xiang, Z. Yuan, Y. Yang, W. Cui, X. Gao, Z. Liu, Y. Jin, B. Sun, Efficient planar heterojunction perovskite solar cells employing graphene oxide as hole conductor. Nanoscale **6**, 10505–10510 (2014)
190. J.-S. Yeo, R. Kang, S. Lee, Y.-J. Jeon, N. Myoung, C.-L. Lee, D.-Y. Kim, J.-M. Yun, Y.-H. Seo, S.-S. Kim, S.-I. Na, Highly efficient and stable planar perovskite solar cells with reduced graphene oxide nanosheets as electrode interlayer. Nano Energy **12**, 96–104 (2015)
191. T. Liu, D. Kim, H. Han, A.R.B. Mohd Yusoff, J. Jang, Fine-tuning optical and electronic properties of graphene oxide for highly efficient perovskite solar cells. Nanoscale **7**, 10708–10718 (2015)
192. K. Yan, Z. Wei, J. Li, H. Chen, Y. Yi, X. Zheng, X. Long, Z. Wang, J. Wang, J. Xu, S. Yang, High-performance graphene-based hole conductor-free perovskite solar cells: Schottky junction enhanced hole extraction and electron blocking. Small **11**, 2269–2274 (2015)
193. P. You, Z. Liu, Q. Tai, S. Liu, F. Yan, Efficient semitransparent perovskite solar cells with graphene electrodes. Adv. Mater. **27**, 3632–3638 (2015)
194. J. Cao, Y.-M. Liu, X. Jing, J. Yin, J. Li, B. Xu, Y.-Z. Tan, N. Zheng, Well-defined thiolated nanographene as hole-transporting material for efficient and stable perovskite solar cells. J. Am. Chem. Soc. **137**, 10914–10917 (2015)
195. Y. Yang, J. Xiao, H. Wei, L. Zhu, D. Li, Y. Luo, H. Wu, Q. Meng, An all-carbon counter electrode for highly efficient hole-conductor-free organo-metal perovskite solar cells. RSC Adv. **4**, 52825–52830 (2014)
196. F. Zhang, X. Yang, H. Wang, M. Cheng, J. Zhao, L. Sun, Structure engineering of hole-conductor free perovskite-based solar cells with low-temperature-processed commercial carbon paste as cathode. ACS Appl. Mater. Interfaces **6**, 16140–16146 (2014)
197. Z. Ku, Y. Rong, M. Xu, T. Liu, H. Han, Full printable processed mesoscopic $CH_3NH_3PbI_3$/TiO_2 heterojunction solar cells with carbon counter electrode. Sci. Rep., **3** (2013)
198. H. Wang, X. Hu, H. Chen, The effect of carbon black in carbon counter electrode for $CH_3NH_3PbI_3$/TiO_2 heterojunction solar cells. RSC Adv. **5**, 30192–30196 (2015)
199. M. Xu, Y. Rong, Z. Ku, A. Mei, T. Liu, L. Zhang, X. Li, H. Han, Highly ordered mesoporous carbon for mesoscopic $CH_3NH_3PbI_3$/TiO_2 heterojunction solar cell. J. Mater. Chem. A **2**, 8607–8611 (2014)
200. A. Mei, X. Li, L. Liu, Z. Ku, T. Liu, Y. Rong, M. Xu, M. Hu, J. Chen, Y. Yang, A hole-conductor–free, fully printable mesoscopic perovskite solar cell with high stability. Science **345**, 295–298 (2014)
201. Z. Li, S.A. Kulkarni, P.P. Boix, E. Shi, A. Cao, K. Fu, S.K. Batabyal, J. Zhang, Q. Xiong, L.H. Wong, N. Mathews, S.G. Mhaisalkar, Laminated carbon nanotube networks for metal electrode-free efficient perovskite solar cells. ACS Nano **8**, 6797–6804 (2014)
202. S.N. Habisreutinger, T. Leijtens, G.E. Eperon, S.D. Stranks, R.J. Nicholas, H.J. Snaith, Carbon nanotube/polymer composites as a highly stable hole collection layer in perovskite solar cells. Nano Lett. **14**, 5561–5568 (2014)
203. R. Li, X. Xiang, X. Tong, J. Zou, Q. Li, Wearable double-twisted fibrous perovskite solar cell. Adv. Mater. **27**, 3831–3835 (2015)
204. K. Wojciechowski, T. Leijtens, S. Spirova, C. Schlueter, M. Hoerantner, J.T.-W. Wang, C.-Z. Li, A.K.-Y. Jen, T.-L. Lee, H.J. Snaith, C_{60} as an efficient N-type compact layer in perovskite solar cells. J. Phys. Chem. Lett. **6**, 2399–2405 (2015)
205. Y. Li, J. Zhu, Y. Huang, F. Liu, M. Lv, S. Chen, L. Hu, J. Tang, J. Yao, S. Dai, Mesoporous SnO_2 nanoparticle films as electron-transporting material in perovskite solar cells. Rsc Adv. **5**, 28424–28429 (2015)
206. J. Song, E. Zheng, J. Bian, X.-F. Wang, W. Tian, Y. Sanehira, T. Miyasaka, Low-temperature SnO_2-based electron selective contact for efficient and stable perovskite solar cells. J. Mater. Chem. A **3**, 10837–10844 (2015)

207. Q. Dong, Y. Shi, K. Wang, Y. Li, S. Wang, H. Zhang, Y. Xing, Y. Du, X. Bai, T. Ma, Insight into Perovskite solar cells based on SnO_2 compact electron-selective layer. J. Phys. Chem. C **119**, 10212–10217 (2015)
208. M.J. Carnie, C. Charbonneau, M.L. Davies, B.O. Regan, D.A. Worsley, T.M. Watson, Performance enhancement of solution processed perovskite solar cells incorporating functionalized silica nanoparticles. J. Mater. Chem. A **2**, 17077–17084 (2014)
209. S.H. Hwang, J. Roh, J. Lee, J. Ryu, J. Yun, J. Jang, Size-controlled SiO_2 nanoparticles as scaffold Layers in thin-film perovskite solar cells. J. Mater. Chem. A **2**, 16429–16433 (2014)
210. S.S. Shin, W.S. Yang, J.H. Noh, J.H. Suk, N.J. Jeon, J.H. Park, J.S. Kim, W.M. Seong, S.I. Seok, High-performance flexible perovskite solar cells exploiting Zn_2SnO_4 prepared in solution below 100 °C. Nat. Commum. **6**, 7410 (2015)
211. L.S. Oh, D.H. Kim, J.A. Lee, S.S. Shin, J.-W. Lee, I.J. Park, M.J. Ko, N.-G. Park, S.G. Pyo, K.S. Hong, J.Y. Kim, Zn_2SnO_4-based photoelectrodes for organolead halide perovskite solar cells. J. Phys. Chem. C **118**, 22991–22994 (2014)
212. A. Bera, K. Wu, A. Sheikh, E. Alarousu, O.F. Mohammed, T. Wu, Perovskite oxide $SrTiO_3$ as an efficient electron transporter for hybrid perovskite solar cells. J. Phys. Chem. C **118**, 28494–28501 (2014)
213. A. Kogo, Y. Numata, M. Ikegami, T. Miyasaka, Nb_2O_5 blocking layer for high open-circuit voltage perovskite solar cells. Chem. Lett. **44**, 829–830 (2015)
214. L. Hu, W. Wang, H. Liu, J. Peng, H. Cao, G. Shao, Z. Xia, W. Ma, J. Tang, PbS colloidal quantum dots as an effective hole transporter for planar heterojunction perovskite solar cells. J. Mater. Chem. A **3**, 515–518 (2015)
215. M. Lv, J. Zhu, Y. Huang, Y. Li, Z. Shao, Y. Xu, S. Dai, Colloidal $CuInS_2$ quantum dots as inorganic hole-transporting material in perovskite solar cells. ACS Appl. Mater. Interfaces **7**, 17482–17488 (2015)
216. Q. Hu, J. Wu, C. Jiang, T. Liu, X. Que, R. Zhu, Q. Gong, Engineering of electron-selective contact for perovskite solar cells with efficiency exceeding 15 %. ACS Nano **8**, 10161–10167 (2014)
217. Y. Zhao, A.M. Nardes, K. Zhu, Effective hole extraction using MoO_x-Al contact in perovskite $CH_3NH_3PbI_3$ solar cells. Appl. Phys. Lett., **104**, (2014)
218. F. Hou, Z. Su, F. Jin, X. Yan, L. Wang, H. Zhao, J. Zhu, B. Chu, W. Li, Efficient and stable planar heterojunction perovskite solar cells with an MoO_3/PEDOT:PSS hole transporting layer. Nanoscale **7**, 9427–9432 (2015)
219. J.A. Christians, R.C.M. Fung, P.V. Kamat, An inorganic hole conductor for organo-lead halide perovskite solar cells. Improved hole conductivity with copper iodide. J. Am. Chem. Soc. **136**, 758–764 (2014)
220. S. Chavhan, O. Miguel, H.-J. Grande, V. Gonzalez-Pedro, R.S. Sanchez, E.M. Barea, I. Mora-Sero, R. Tena-Zaera, Organo-metal halide perovskite-based solar cells with CuSCN as the inorganic hole selective contact. J. Mater. Chem. A **2**, 12754–12760 (2014)
221. S. Ye, W. Sun, Y. Li, W. Yan, H. Peng, Z. Bian, Z. Liu, C. Huang, CuSCN-based inverted planar perovskite solar cell with an average PCE of 15.6. Nano Lett. **15**, 3723–3728 (2015)
222. S. Ito, S. Tanaka, H. Vahlman, H. Nishino, K. Manabe, P. Lund, Carbon-double-bond-free printed solar cells from TiO_2/$CH_3NH_3PbI_3$/CuSCN/Au: structural control and photoaging effects. ChemPhysChem **15**, 1194–1200 (2014)

http://www.springer.com/978-3-319-32021-2

Nanomaterials for Sustainable Energy
Li, Q. (Ed.)
2016, XVII, 590 p. 292 illus., 36 illus. in color.,
Hardcover
ISBN: 978-3-319-32021-2